




Cite this: *RSC Adv.*, 2025, 15, 37391

# Design, synthesis and SAR of novel naphthalene-sulfonamide hybrids: anticancer assessment, gene expression analysis of IL6/JAK2/STAT3 signaling in MCF7 cells and antimicrobial evaluation

Ghada H. Elsayed,<sup>ab</sup> Nagwa M. Abdelazeem,<sup>c</sup> Alaa M. Saleh,<sup>d</sup> Sherein Abd El-Moez,<sup>e</sup> Marwa El-Hussieny <sup>\*c</sup> and Aisha A. K. Al-Ashmawy <sup>\*f</sup>

A multi-target and molecular hybridization drug design approach was used in the design and synthesis of novel 6-acetylnaphthalene-2-sulfonamide derivatives (**5a–5j**) for anticancer and antimicrobial evaluation. The compounds **5a**, **5b**, **5e**, and **5i** revealed the most cytotoxic activity against the human breast cancer cell line (MCF7) with a good safety profile against the normal Madin–Darby canine kidney cell line (MDCK). Compounds **5b** and **5i** exhibited significant antiproliferative activity in MCF7 cells by downregulating IL6, JAK2, STAT3, BCL2, Cyclin D1, and c-MYC, while upregulating BAX expression levels, relative to control values, as confirmed by qRT-PCR analysis. Moreover, the antibacterial and anti-mycotic activities for **5a–5j** were assessed, and the minimum inhibitory concentration (MIC) was evaluated for the promising compounds. In *in vitro* enzymatic assays, compounds **5e** and **5b** potently inhibited STAT3 phosphorylation with  $IC_{50} = 3.01 \mu M$  and  $3.59 \mu M$ , respectively, compared with cryptotanshinone ( $IC_{50} = 3.52 \mu M$ ); compound **5b** potently inhibited topoisomerase IV ( $IC_{50} = 5.3 \mu g mL^{-1}$ , norfloxacin  $IC_{50} = 8.24 \mu g mL^{-1}$ ) and moderately inhibited DNA gyrase in *E. coli*; and compound **5e** effectively inhibited topoisomerase IV ( $IC_{50} = 7.65 \mu g mL^{-1}$ , norfloxacin  $IC_{50} = 7.07 \mu g mL^{-1}$ ) and moderately inhibited DNA gyrase in *S. aureus*. Finally, SAR was discussed, revealing the essential role of the *N*-aryl and/or heteroaryl moiety in directing the biological activity of each compound towards a specific target. An *in silico* study was performed to predict ADME and docking for the promising hybrids. Collectively, the 6-acetylnaphthalene-2-sulfonamide hybrids suppressed MCF7 cell proliferation and induced apoptosis *via* modulation of the IL6/JAK2/STAT3 signaling pathway and representing promising building blocks as STAT3 inhibitors and antimicrobial leads for future modifications.

Received 26th July 2025  
Accepted 5th September 2025

DOI: 10.1039/d5ra05413c

rsc.li/rsc-advances

## 1 Introduction

Global cancer statistics (GLOBOCAN) 2020 estimates that the incidence of cancer would increase by around 47% in 2040 compared to cases reported in 2020. The cancer mortality rate would most likely rise in tandem with the growing number of

cases, especially those related to colorectal and breast cancers.<sup>1</sup> The IL6/JAK2/STAT3 signalling pathway is closely linked to the development and progression of many human tumours, including gastric cancer,<sup>2</sup> breast cancer,<sup>3</sup> liver cancer,<sup>4</sup> colorectal cancer,<sup>5</sup> colon cancer,<sup>6</sup> ovarian cancer,<sup>7</sup> lung cancer,<sup>8</sup> and pancreatic cancer.<sup>9</sup> A pleiotropic factor, interleukin 6 (IL6), is reported to have physiological and pathological roles in immunology, inflammation, and cancer.<sup>10</sup> It can trigger the overexpression of STAT3 (signal transducer and activator of transcription 3) and JAK2 (Janus kinase 2), consequently activating downstream effector molecules and resulting in the proliferation, differentiation, cell survival, invasiveness, inhibition of apoptosis, and growth of cancer cells.<sup>11</sup> The BCL2 and BAX proteins are critical for controlling apoptosis. In breast cancer, an elevated level of BCL2 promotes cell survival by suppressing apoptosis, whereas an increase in BAX causes cell death.<sup>12</sup> c-MYC, a transcription factor, is over-expressed in solid and hematologic tumors and affects proteins such as caspase 3, BAX, and BCL2, which control the development of tumors and

<sup>a</sup>Hormones Department, Medical Research and Clinical Studies Institute, National Research Centre, Dokki, Cairo, 12622, Egypt

<sup>b</sup>Stem Cell Lab, Centre of Excellence for Advanced Sciences, National Research Centre, Dokki, Cairo, 12622, Egypt

<sup>c</sup>Organometallic and Organometaloid Chemistry Department, National Research Centre, Dokki, Cairo, 12622, Egypt. E-mail: me.awad@nrc.sci.eg; mrw\_elhussieny@yahoo.com

<sup>d</sup>Chemistry of Natural and Microbial Products Department, Pharmaceutical and Drug Industries Research Institute, National Research Centre, Dokki, Cairo, 12622, Egypt

<sup>e</sup>Microbiology and Immunology Department, Veterinary Research Institute, National Research Centre, Dokki, Cairo, 12622, Egypt

<sup>f</sup>Department of Therapeutic Chemistry, Pharmaceutical and Drug Industries Research Institute, National Research Centre, Dokki, Cairo, 12622, Egypt. E-mail: aisha\_pharmacy@yahoo.com; aa.al-ashmawy@nrc.sci.eg



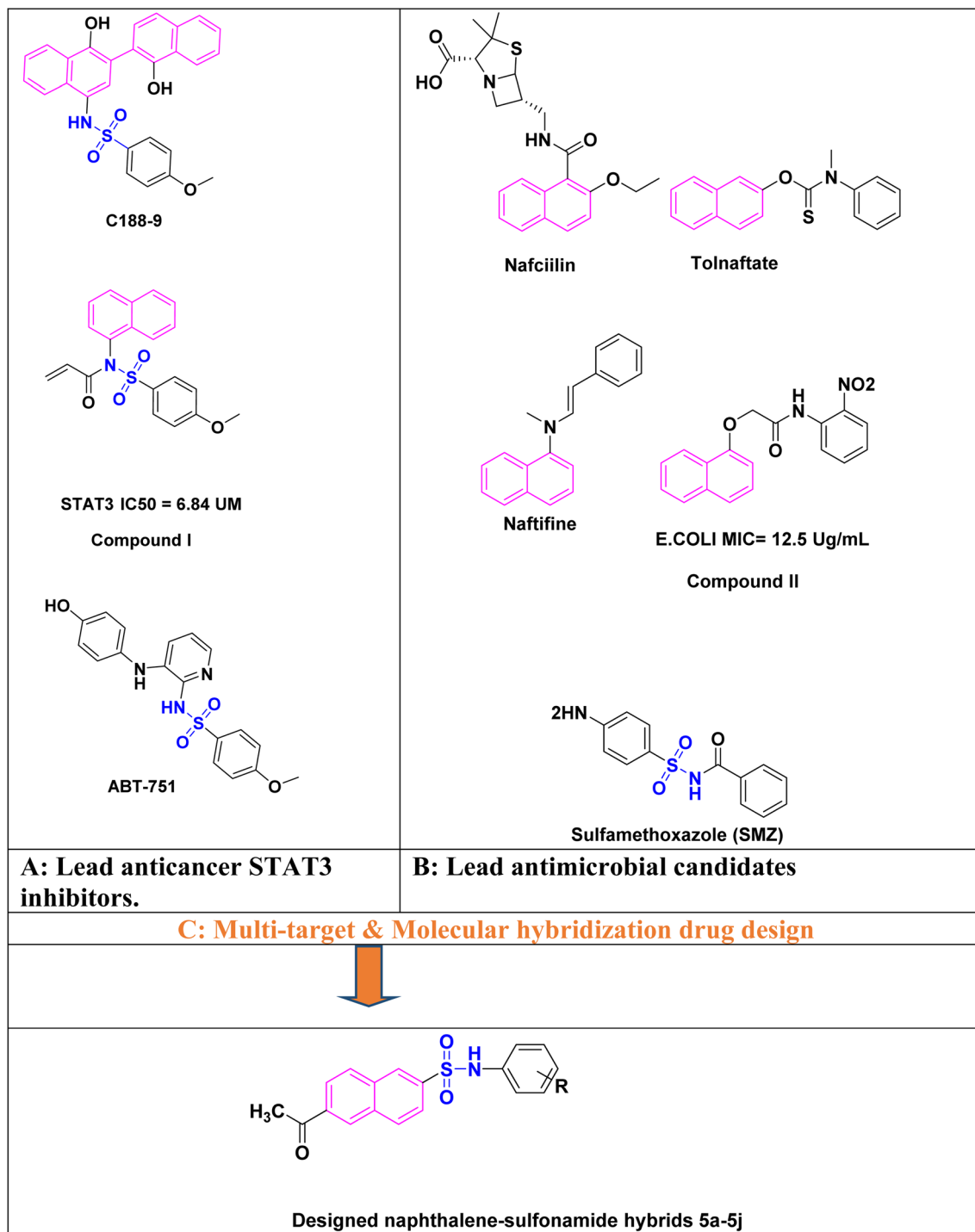


Fig. 1 (A) Reported lead anticancer STAT3 inhibitors; (B) reported lead antimicrobial candidates; (C) multitarget and molecular hybridization drug design to develop the designed naphthalene-sulfonamide hybrids 5a-5j.

apoptotic cell death.<sup>13-15</sup> Cyclin D1 protein is associated with the proliferation of cancer and functions as a regulator of the cell cycle (G1 to S phase progression). One of Cyclin D1's binding partners, cyclin dependent kinase 4 (CDK4), helps create active complexes that advance the cell cycle.<sup>16,17</sup> Since over-activation of STAT3 may participate in the cell cycle and survival, it can up-regulate Cyclin D1, c-MYC, and BCL2 to inhibit the apoptosis of breast cancer cells.<sup>18</sup> Furthermore, BAX/BCL2-related

caspase-dependent apoptosis can be inhibited by STAT3 triggered by the IL6/JAK2 pathway.<sup>19</sup> From previously reported clinical and preclinical data, the overexpression of STAT3 was involved in metastasis and chemoresistance of breast cancer.<sup>20</sup> Therefore, the development of new compounds as STAT3 inhibitors could be a promising therapeutic approach for breast cancer treatment.



The chaotic use of antibiotics has led to the emergence of antimicrobial drug resistance (AMDR), which is a serious worldwide health concern.<sup>21</sup> The World Health Organization (WHO) reported on calls for urgent action to face the disastrous AMDR, which may lead to 10 million deaths yearly by 2050.<sup>22</sup> Moreover, the WHO published a list of antibiotic-resistant priority pathogens to highlight the importance of antimicrobial research and development.<sup>23</sup> Consequently, there is a pressing need to develop new antimicrobial compounds to address AMDR problems. Type IIA topoisomerases, such as bacterial DNA gyrase and topoisomerase IV, alter DNA topology by cleaving the two strands of the double helix during bacterial cell division. Gyrase is essential in the supercoiling of the chromosomal DNA, while topoisomerase IV is responsible for the segregation of the bacterial genetic material into two newly formed daughter cells. Consequently, inhibitors of both enzymes are considered attractive antibacterial candidates due to the absence of these enzymes in eukaryotes and their well-known mechanism of action in bacterial division.<sup>24</sup>

Naphthalene, a bicyclic aromatic ring, is derived from coal tar as a white crystalline solid with a strong odor. Its formula was first reported by Michael Faraday.<sup>25</sup> Naphthalene can be synthesized chemically by Diels–Alder reaction of maleic anhydride, followed by decarboxylation.<sup>26</sup> A literature survey revealed that naphthalene-containing compounds have a wide range of pharmacological activities such as anticancer,<sup>27</sup> antimicrobial,<sup>28</sup> antiviral,<sup>29</sup> anti-inflammatory,<sup>30</sup> and anti-neurodegenerative properties.<sup>31</sup> A bis-naphthalene-4-methoxybenzenesulfonamide candidate, C188-9, is a potent STAT3 inhibitor in phase I/II clinical trial that is used for head and neck squamous cell carcinoma.<sup>32</sup> Also, a sulfonyl-*N*-(naphthalene-1-yl)acrylamide derivative (compound **I**) was reported as a potent STAT3 inhibitor ( $IC_{50} = 6.84 \mu M$ ) with a promising antiproliferative activity against A549 ( $IC_{50} = 1.35 \mu M$ ), HCT-116 ( $IC_{50} = 3.04 \mu M$ ) and MDA-MB-231 ( $IC_{50} = 2.85 \mu M$ ) cells.<sup>33</sup> Some examples of naphthalene-containing FDA-approved drugs in the antimicrobial field include nafcillin, which is a narrow-spectrum beta-lactam antibiotic,<sup>34</sup> tolnaftate, which is a squalene epoxidase inhibitor marketed as an antifungal drug,<sup>35</sup> and naftifine, which is an antifungal medication that is used topically.<sup>36</sup> In 2022, Yadav and coworkers reported on an amide-coupled naphthalene derivative (compound **II**) as a potent broad-spectrum antimicrobial with a minimum inhibitory concentration (MIC) of  $12.5 \mu g mL^{-1}$  and  $62.5 \mu g mL^{-1}$  against *E. coli* and *S. aureus*, respectively.<sup>37</sup> Sulfonamides are well known for a wide range of therapeutic activities such as anticancer,<sup>38</sup> antibacterial,<sup>39</sup> antifungal,<sup>40</sup> anti-inflammatory, and anti-HIV.<sup>41</sup> ABT-751 is an orally bioavailable sulfonamide candidate in phase II clinical trial with a promising effect against lung, breast, and colon cancers. It mainly inhibits tubulin polymerization and weakly inhibits STAT3 phosphorylation.<sup>42</sup> Sulfamethoxazole (SMZ) is an example of sulfonamides in the market. This class of antibiotics blocks bacterial folic acid synthesis by competing with *p*-aminobenzoic acid (PABA) in dihydropteroate synthase (DHPS).<sup>43</sup> The multi-target drug design approach is effective in complicated diseases with complex cross-linked pathways. It can be

considered as an attempt to avoid multiple drug administration, and/or to expect a synergistic therapeutic effect.<sup>44,45</sup> Moreover, the molecular hybridization of two or more active structural moieties may augment the biological activity against a specific target.<sup>46</sup>

According to the aforementioned findings, in this study, a structural modification of the previously reported naphthalene-sulfonamide hybrids (C188-9, compound **I** and ABT-751) as STAT3 inhibitors was carried out, such as introducing a 6-acetyl moiety and inserting different substituted aryl and heteroaryl sulfonamides at position 2 of the naphthalene core structure as shown in Fig. 1. Then, the cytotoxic activity of the new compounds against MCF7 cancer cells and MDCK normal cells was evaluated. Also, the gene expression levels of IL6, JAK2, STAT3, BCL2, BAX, Cyclin D1, and c-MYC in MCF7 cells were assessed. On the other hand, the structural hybridization of the naphthalene core with a sulphonamide moiety was newly used for antimicrobial screening against Gram-negative reference strains; *E. coli*, Gram-positive reference strains; *S. aureus*, and mycotic reference strain/isolate, including yeast; *C. albicans* and mould isolate; *A. flavus* by agar disc diffusion test (ADDT). The minimum inhibitory concentration (MIC) was determined for the promising compounds. Then, *in vitro* enzymatic assays of the active compounds were performed against STAT-3, *E. coli* (DNA gyrase/topoisomerase IV), and *S. aureus* (DNA gyrase/topoisomerase IV). Finally, a molecular docking study was performed to predict the best binding pose and interaction of the active compounds against the target proteins.

## 2 Results and discussion

### 2.1. Chemistry

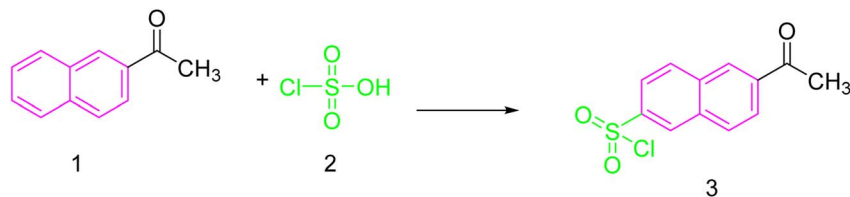
Firstly, we prepared 6-acetylnaphthalene-2-sulfonyl chloride (**3**) from the reaction of 1-naphthalen-2-yl ethanone (**1**) with chlorosulfonic acid (**2**) (Scheme 1).

Then, we studied the reaction of 6-acetylnaphthalene-2-sulfonyl chloride (**3**) with the desired amines **4** in dichloromethane to form 6-acetyl-*N*-phenylnaphthalene-2-sulfonamide derivatives **5a–j**. The chemical structures of **5a–j** were confirmed using microanalyses and several spectroscopic data (Scheme 2).

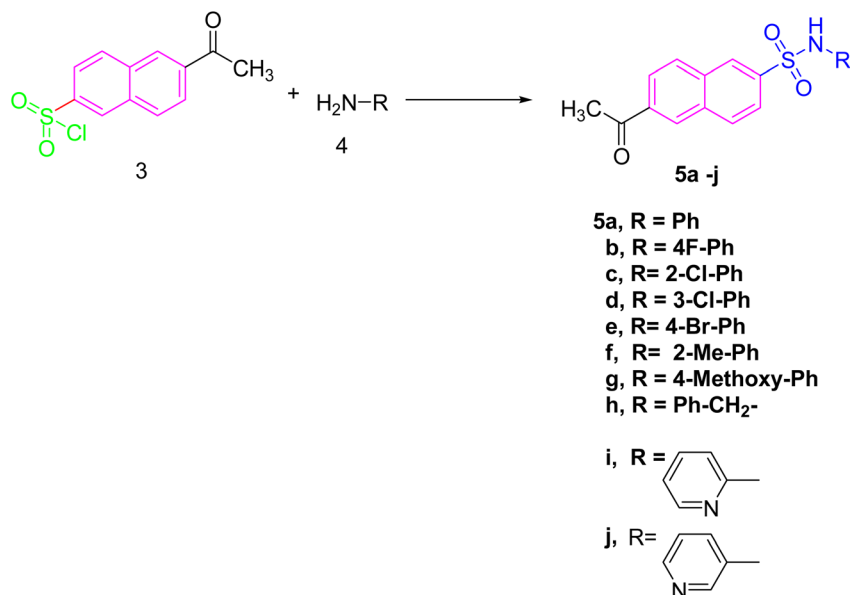
### 2.2. Biological evaluation

**2.2.1. Cytotoxic effect of the synthesized compounds.** The neutral red assay, which is based on the ability of viable cells to incorporate and bind the supravital dye neutral red in the lysosomes, was used to assess the *in vitro* cytotoxicity of the synthesized compounds (**5a–5j**) against the cancer cell line MCF7 and the normal cell line MDCK at various concentrations from 12.5 to 100  $\mu M$ . As a reference drug, doxorubicin (Dox) had a significant impact on the growth of MCF7 and MDCK cells after 48 hours when compared to untreated cells. The viability of MCF7 and MDCK cells was not significantly affected by the use of DMSO as a solvent after a 48 hour treatment. The cytotoxic activity of the compounds was evaluated against the MCF7 and MDCK cell lines. The  $IC_{50}$  values and selectivity index (SI)





Scheme 1 Preparation of 6-acetylnaphthalene-2-sulfonyl chloride.



Scheme 2 Synthesized 6-acetyl-N-phenylnaphthalene-2-sulfonamide derivatives.

obtained from the neutral red assay are presented in Table 1, Fig. 2A, B and 3A, B. After 48 h of incubation time, compounds **5a**, **5b**, **5e**, and **5i** with IC<sub>50</sub> values of 42.13, 40.08, 43.13, and 41.6 μM, respectively, revealed more cytotoxicity on the MCF7-

treated cells compared with the untreated cells ( $P > 0.05$ ). The IC<sub>50</sub> values of 42.13, 40.08, 43.13, and 41.6 μM and IC<sub>50</sub> values of 90.9, 93.4, 95.8, and 88.8 μM for compounds **5a**, **5b**, **5e**, and **5i** in the MCF7 cells and the MDCK cells, respectively, were used to determine the selectivity indexes (SI) of each compound, which represents the overall activity. The degree of selectivity of the compounds can be expressed by their Selectivity Index (SI) value. Selectivity of the cytotoxic effect of the tested compounds was determined by comparing the cytotoxic activity (IC<sub>50</sub>) of each compound against the cancerous MCF7 cells with the normal MDCK cells. Significant SI values were observed for all investigated compounds: 2.15, 2.33, 2.22, and 2.13 for **5a**, **5b**, **5e**, and **5i** on MCF7 cells, respectively. These findings showed that the tested compounds **5a**, **5b**, **5e**, and **5i** had the most promising cytotoxic action on the MCF7 breast cancer cells.

**2.2.1.1 Structure-activity relationship (SAR).** The combination of various heterocyclic rings to the 6-acetylnaphthalene-2-sulfonyl chloride moiety appears to have led to alterations in the cytotoxic activity of these compounds in MCF7 cells, according to the structure-activity relationship study. After a 48 hour incubation, the addition of a phenyl ring to 6-acetylnaphthalene-2-sulfonyl chloride to give compound **5a** is more efficient and potent than the addition of *o*-tolyl, methoxyphenyl, and benzyl rings to 6-acetylnaphthalene-2-

Table 1 Cytotoxic activity expressed as IC<sub>50</sub> (μM) of the new derivatives<sup>a</sup>

Compounds no.	IC <sub>50</sub> (μM)		(SI)*
	MCF7	MDCK	MCF7
<b>5a</b>	42.13*	90.9	2.15
<b>5b</b>	40.08*	93.4	2.33
<b>5c</b>	ND	12.65*	ND
<b>5d</b>	ND	ND	ND
<b>5e</b>	43.13*	95.8	2.22
<b>5f</b>	ND	21.8*	ND
<b>5g</b>	ND	18.2*	ND
<b>5h</b>	ND	ND	ND
<b>5i</b>	41.6*	88.8	2.13
<b>5j</b>	ND	20.7*	ND
Doxorubicin	22.8*	70.05*	3.07

<sup>a</sup> IC<sub>50</sub>: concentration needed to reduce the viability of cells by 50%. \* (SI) = IC<sub>50</sub> MDCK cell/IC<sub>50</sub> MCF7 cell. ND: means not detected within the range of the tested concentrations. \* significant difference from the control values at  $P > 0.05$ .



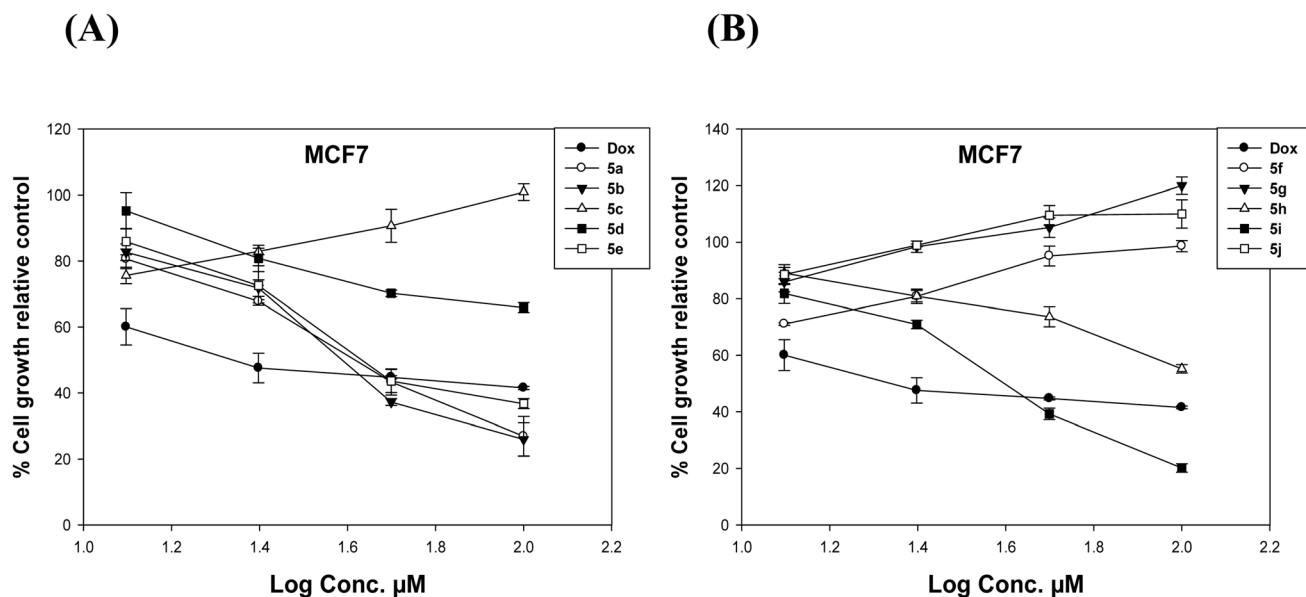


Fig. 2 (A and B) The impact of the tested compounds on MCF7 cells after 48 h.

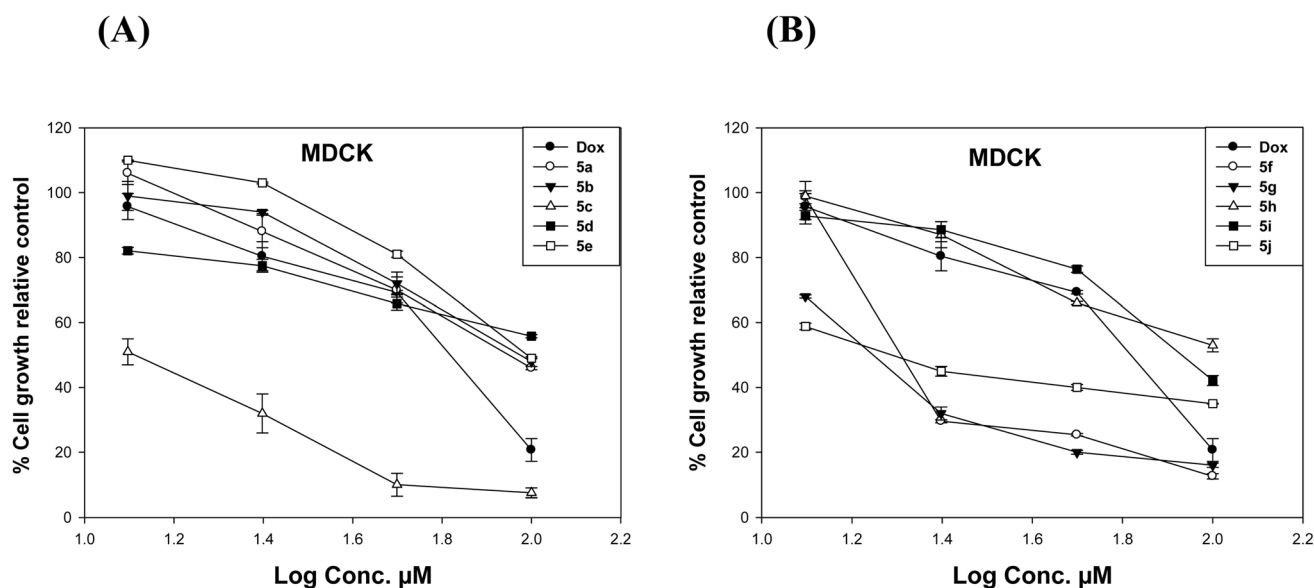


Fig. 3 (A and B) The impact of the tested compounds on MDCK cells after 48 h.

sulfonyl chloride to give compounds **5f**, **5g**, and **5h**, respectively. The phenyl moiety in hybrid **5a** has a mild ( $-I$ ) inductive effect and no resonance effect, so the net electronic effect is neutral. Concerning the steric effect, it is planar with moderate bulkiness. Compounds **5b** and **5e** have 4-fluoro and 4-bromophenyl groups, which are more cytotoxic than compounds **5c** and **5d**, which contain 2- and 3-chlorophenyl groups, respectively. Therefore, it is obvious that the *para* substitution of the phenyl moiety with halogen is preferred for anticancer activity compared to the *ortho* or *meta* halogen substitution. In hybrid **5b**, the high electronegativity of the fluorine atom resulted in a strong electron-withdrawing inductive effect ( $-I$ ), which is

opposed by the electron-donating resonance effect due to its lone pairs ( $+R$ ) that ended up with a slight electron withdrawing effect. In the case of the **5e** hybrid, the 4-bromophenyl group having moderate ( $-I$ ) and strong ( $+R$ ) ended up with a net electron-withdrawing group, but was weaker than the 4-fluoro moiety. As a result of the fluorine atom being small, 4-fluorophenyl had the same steric bulkiness as the unsubstituted phenyl. However, the 4-bromophenyl was slightly more sterically hindered than **5a** and **5b** due to the large size of the bromine atom. Additionally, the existence of the pyridine-2-yl ring in compound **5i** had a greater effect than the existence of the pyridine-3-yl ring in compound **5j**. The pyridine has

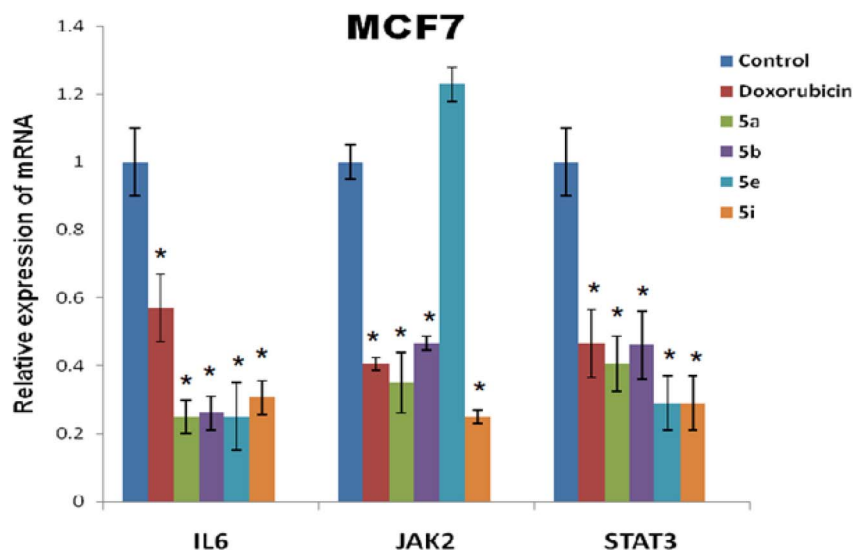


Fig. 4 Effects of doxorubicin and the investigated derivatives on the MCF7 cell gene expression levels of IL6, JAK2, and STAT3. The data were reproducible and are shown as the mean  $\pm$  SEM with  $*P < 0.05$ .

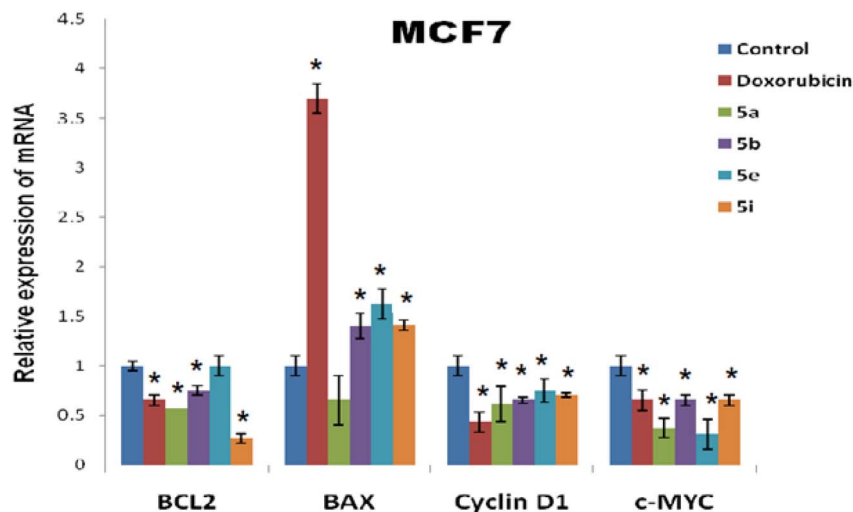


Fig. 5 Effects of doxorubicin and the investigated derivatives on the MCF7 cell gene expression levels of BCL2, BAX, Cyclin D1, and c-MYC. The data were reproducible and are shown as the mean  $\pm$  SEM with  $*P < 0.05$ .

a strong electron-withdrawing inductive effect ( $-I$ ) and it is sterically similar to the phenyl size. Therefore, our findings demonstrated the impact of phenyl, 4-fluorophenyl, 4-bromophenyl, and pyridin-2-yl rings as pharmacophores for the anti-tumor action.

**2.2.2. Gene expression findings.** One of the main causes of death for women is breast cancer. Extensive attempts have been made in the last several decades to determine the pathogenesis of breast cancer.<sup>10</sup> IL6 is one of the best-studied pro-tumorigenic cytokines due to its important involvement in pathological and physiological processes.<sup>47</sup> In breast cancer, a signal transduction hexameric receptor complex is formed when the IL6 binds to its receptor in association with glycoprotein 130 (gp130). This interaction recruits and activates

Janus kinases (JAKs), leading to phosphorylation of STAT3 and subsequent regulation of downstream target genes.<sup>48</sup> The JAK/STAT signaling pathway is one of the main signaling cascades that facilitate cancer cell survival and proliferation.<sup>49</sup>

In breast tumor cells, the over-activated STAT3 upregulates the target genes Cyclin D1, c-MYC, MCL1, and BCL2, which leads to tumor growth and inhibition of apoptosis.<sup>50–52</sup> On the other hand, the over-activated STAT3 may also suppress the production of proteins that promote apoptosis and participate in the initiation and/or acceleration of apoptosis, such as Fas,<sup>53</sup> BAX,<sup>54</sup> and P53.<sup>55</sup> Constitutively active IL6/JAK/STAT3 signaling inhibits apoptosis while promoting the growth and invasiveness of cancer cells.<sup>56</sup> Moreover, a literature survey revealed that MCF7 cells downregulate the expression of BAX and upregulate





Table 2 Zone of inhibition of the tested compounds using the agar well diffusion test (AWDT)<sup>a</sup>

Tested strains	Tested compounds									
	5a	5b	5c	5d	5e	5f	5g	5h	5i	5j
<i>S. aureus</i> ATCC 25923 (1)	0 (–)	0 (–)	0 (–)	0 (–)	16 (+++)	0 (–)	0 (–)	14 (++)	0 (–)	0 (–)
<i>E. coli</i> O157 ATCC 700728 (2)	10 S (+)	15 (+++)	12 (++)	10 (+)	12 (++)	11 (+)	12 (++)	10 (+)	11 (+)	16 (+++)
<i>C. albicans</i> ATCC 10231 (3)	12 (++)	15 (+++)	16 (+++)	15 (+)	15 (+++)	12 (+)	10 (+)	7 (+)	14 (+)	16 (+++)
<i>A. flavus</i> isolate (4)	0 (–)	0 (–)	0 (–)	0 (–)	11 (+)	0 (–)	0 (–)	10 (+)	0 (–)	7 (+)

<sup>a</sup> Key of inhibition scale: negative inhibition “zero” (0), 0–6 mm (–), 7–11 mm (+), 12–14 mm (++) , 15–17 mm (+++). S bacteriostatic antimicrobial activity.

Table 3 Minimum inhibitory concentration (MIC) of the promising compounds

Strains	Compound	MIC (mg mL <sup>−1</sup> )
<i>E. coli</i> O157 ATCC 700728	5b	10
<i>E. coli</i> O157 ATCC 700728	5j	20
<i>S. aureus</i> ATCC 25923	5e	20
<i>S. aureus</i> ATCC 25923	5h	40
<i>C. albicans</i> ATCC 10231	5b	10
<i>C. albicans</i> ATCC 10231	5c	20
<i>C. albicans</i> ATCC 10231	5d	10
<i>C. albicans</i> ATCC 10231	5e	20
<i>C. albicans</i> ATCC 10231	5i	40
<i>C. albicans</i> ATCC 10231	5j	10

the expression of IL6, JAK2, STAT3, BCL2, Cyclin D1, and c-MYC genes.<sup>57–61</sup>

After 48 hours, the IC<sub>50</sub> values of compounds 5a, 5b, 5e, and 5i were used to assess the impact of these compounds on the mRNA expression levels of IL6, JAK2, STAT3, BCL2, BAX, Cyclin D1, and c-MYC genes in MCF7 cells. Additionally, the ratio of its expression to that of β-Actin was calculated in comparison to the control values.

The present research demonstrated that, in MCF7 cells relative to untreated cells, doxorubicin significantly raised the expression levels of the BAX gene while significantly decreasing the expression levels of the IL6, JAK2, STAT3, BCL2, Cyclin D1, and c-MYC genes ( $P > 0.05$ ) (Fig. 4 and 5). Additionally, treatment of MCF7 cells with compounds 5b and 5i resulted in a significant increase in the BAX expression levels relative to the control values and a significant decrease in the expression levels of IL6, JAK2, STAT3, BCL2, Cyclin D1, and c-MYC genes ( $P >$

0.05). Similarly, when compared to control values, compound 5a significantly decreased the expression levels of IL6, JAK2, STAT3, BCL2, and c-MYC in the MCF7 cell line. Compound 5e also caused a significant reduction in the genes for IL6, STAT3, Cyclin D1, and c-MYC ( $P > 0.05$ ). On the other hand, compared to the control values, compound 5e significantly increased the BAX gene in MCF7 cells ( $P > 0.05$ ) (Fig. 4 and 5). These findings are consistent with prior research; the most effective action was shown by SMY002, a naphthalene–SERM hybrid that could directly engage with the SH2 domain of STAT3 and significantly reduce its phosphorylation, dimerisation, nuclear distribution, transcriptional activity, and target gene expression. Additionally, *via* downregulating the expression of Cyclin D1 and MMP9, SMY002 significantly inhibited the migration, invasion, survival, growth, and metastasis of TNBC cells both *in vitro* and *in vivo*.<sup>62</sup> In addition, Minus *et al.*<sup>63</sup> stated that naphthalene sulfonamides are interesting lead chemicals for inhibiting STAT3. These segments function as a flexible core for ligand synthesis and have been demonstrated to bind STAT3. Because of the substituent flexibility of the scaffold, particularly at the 2-, 5-, and 8-positions, halogens or other groups might be added to improve binding or provide redox activity. Fluorinated naphthalene sulfonamides synthesized using modular techniques are one option, emphasizing the significance of halogen substitution for adjusting steric and electronic properties.

The results reported here indicate that compounds 5b and 5i had significant effects by downregulating the levels of IL6, JAK2, STAT3, BCL2, Cyclin D1, and c-MYC and upregulating the BAX gene, which in turn causes apoptosis and inhibits the proliferation of breast cancer cells (MCF7).

**2.2.3. Antimicrobial screening of the synthesized compounds.** The final compounds 5a–5j were individually tested against a variety of certified reference strains, including Gram-negative *E. coli* O157 ATCC 700728, Gram-positive *S. aureus* ATCC 25923, and mycotic reference strain/isolate, including yeast; *C. albicans* ATCC 10231, and mould isolate; *A. flavus* using the Agar Well Diffusion Test (AWDT).<sup>64</sup> After incubation time, antimicrobial activities were expressed as inhibition diameter zones in millimeters (mm). The experiment was carried out in triplicate, and the average zone of inhibition was calculated. The zone of inhibition was measured using a measuring caliper (the detailed method is included in the SI file S3). The results are summarized in Table 2.

From the preliminary antimicrobial screening, the promising compounds were chosen to investigate their minimum

Table 4 IC<sub>50</sub> values of the four tested compounds 5a, 5b, 5e, and 5i as STAT3 phosphorylation inhibitors

Compounds		STAT3 phosphorylation IC <sub>50</sub> (μM) (mean ± SD)
1	5a	7.87 ± 0.74 <sup>a</sup>
2	5b	3.59 ± 0.70
3	5e	3.01 ± 0.06
4	5i	8.58 ± 0.90 <sup>a</sup>
5	Cryptotanshinone	3.52 ± 0.75

<sup>a</sup> Significant difference from cryptotanshinone values at  $P > 0.05$ .



**Table 5** IC<sub>50</sub> values (μg mL<sup>-1</sup>) of **5b** and **5e** against *E. coli* and *S. aureus* DNA gyrase and topoisomerase IV enzymes<sup>a</sup>

IC <sub>50</sub> ± SEM					
Compounds	Organism	DNA gyrase		Topo-IV	
	<i>E. coli</i>	Supercoiling μg mL <sup>-1</sup>	ATPase μg mL <sup>-1</sup>	Cleavage μg mL <sup>-1</sup>	ATPase μg mL <sup>-1</sup>
<b>5b</b>		7.07 ± 0.24 <sup>a</sup>	1.23 ± 0.022 <sup>a</sup>	5.3 ± 0.462	1.2 ± 0.03 <sup>a</sup>
Ref.		Nor 3.56 ± 0.07	Cipro 0.64 ± 0.04	Nor 8.24 ± 0.18	Cipro 0.64 ± 0.07
IC <sub>50</sub> ± SEM					
Compounds	Organism	DNA gyrase		Topo-IV	
	<i>S. aureus</i>	Supercoiling μg mL <sup>-1</sup>	ATPase μg mL <sup>-1</sup>	Decatenation μg mL <sup>-1</sup>	ATPase μg mL <sup>-1</sup>
<b>5e</b>		8.83 ± 0.46 <sup>a</sup>	1.23 ± 0.019 <sup>a</sup>	7.65 ± 0.28	2.41 ± 0.056 <sup>a</sup>
Ref.		Nor 3.56 ± 0.07	Cipro 0.65 ± 0.09	Nor 7.07 ± 0.35	Cipro 0.65 ± 0.012

<sup>a</sup> Significant difference from reference values at *P* > 0.05.**Table 6** Swiss ADME prediction of the drug likeness (Lipinski's rule) with other physicochemical properties, including lipophilicity (MLOGP) and water solubility (Ali log *S*) for compounds **5a–5j**<sup>a</sup>

Compounds	Lipinski rules						Violation	Water solubility	
	MW (g mol <sup>-1</sup> )	HBA	HBD	TPSA	MLOGP	Rotatable (bonds ≤ 9)	Yes or 0	Ali log <i>S</i>	Ali class
<b>5a</b>	325.38	3	1	71.62	2.6	4	0	−4.59	Moderate
<b>5b</b>	343.37	4	1	71.62	2.99	4	0	−4.67	Moderate
<b>5c</b>	359.83	3	1	71.62	3.1	4	0	−4.8	Moderate
<b>5d</b>	359.83	3	1	71.62	3.1	4	0	−5.22	Moderate
<b>5e</b>	404.28	3	1	71.62	3.22	4	0	−5.28	Moderate
<b>5f</b>	339.41	3	1	71.62	2.83	4	0	−4.83	Moderate
<b>5g</b>	355.41	4	1	80.85	2.27	5	0	−4.73	Moderate
<b>5h</b>	339.41	4	1	71.62	2.57	5	0	−4.5	Moderate
<b>5i</b>	326.37	4	1	84.51	1.14	4	0	−3	Soluble
<b>5j</b>	326.37	4	1	84.51	1.14	4	0	−3.72	Soluble

<sup>a</sup> MW: molecular weight ≤ 500; log *P*: lipophilicity < 4.15; HBA: hydrogen bond acceptor ≤ 10; HBD: hydrogen bond donor ≤ 5; TPSA (topological polar surface area), Ali log *S* scale values ranging from ≤10 (insoluble) to ≤2 (soluble).

inhibitory concentration (MIC) against specific strains as follows: **5b** and **5j** against *E. coli*, **5e** and **5f** against *S. aureus*, **5b**, **5c**, **5d**, **5e**, **5i**, and **5j** against *C. albicans* according to the reported method.<sup>65</sup> The results are summarized in Table 3. It was found that the presence of 4-fluorophenyl attached to 6-acetyl naphthalene-2-sulfonamide in **5b** gave the best MIC

**Table 7** The Swiss ADME pharmacokinetic parameters prediction for GIT absorption, BBB permeability, substrate permeability of glycoprotein, and the inhibitory profile against some CYP 450

Compounds	Swiss ADME			Inhibitors of CYP450				
	GI absorption	BBB permeability	Pgp substrate	CYP1A2	CYP2C19	CYP2C9	CYP2D6	CYP3A4
<b>5a</b>	High	No	No	Yes	Yes	Yes	Yes	Yes
<b>5b</b>	High	No	No	Yes	Yes	Yes	No	Yes
<b>5c</b>	High	No	No	Yes	Yes	Yes	No	Yes
<b>5d</b>	High	No	No	Yes	Yes	Yes	No	Yes
<b>5e</b>	High	No	No	Yes	Yes	Yes	No	Yes
<b>5f</b>	High	No	No	Yes	Yes	Yes	No	Yes
<b>5g</b>	High	No	No	Yes	Yes	Yes	Yes	Yes
<b>5h</b>	High	Yes	No	Yes	Yes	Yes	Yes	Yes
<b>5i</b>	High	No	No	Yes	Yes	Yes	No	Yes
<b>5j</b>	High	No	No	Yes	Yes	Yes	Yes	Yes





**Table 8** The predicted binding affinity and 2D binding mode of **5a**, **5b**, **5e**, and **5i** in the STAT3 binding pocket

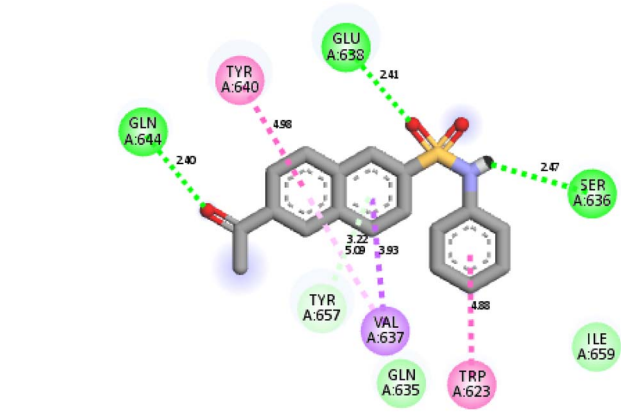
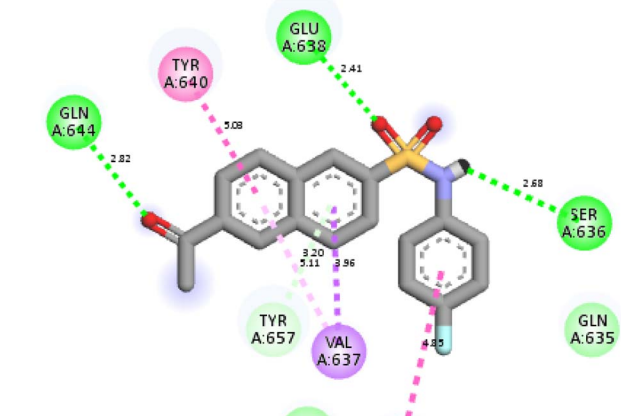
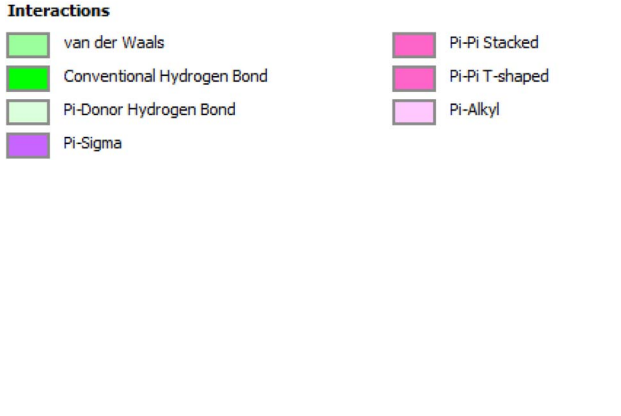
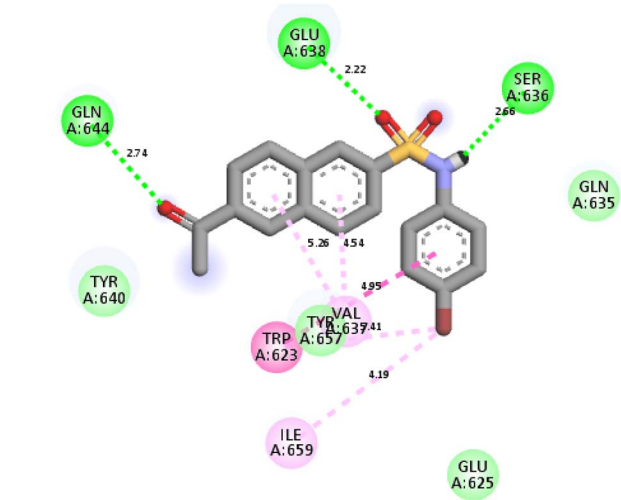
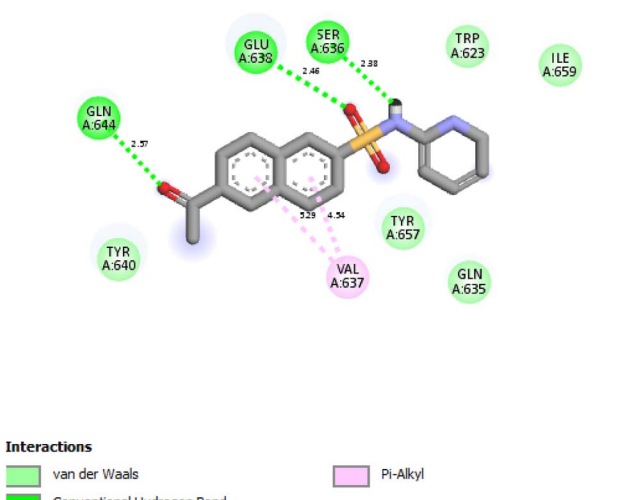
Compound	Binding affinity negative (kcal mol <sup>-1</sup> )	2D predicted binding mode representing the types and measurement of the binding interactions in the STAT-3 binding pocket
<b>5a</b>	−6.6	
<b>5b</b>	−6.7	
<b>5e</b>	−6.7	

Table 8 (Contd.)

Compound	Binding affinity negative (kcal mol <sup>-1</sup> )	2D predicted binding mode representing the types and measurement of the binding interactions in the STAT-3 binding pocket
5i	−6.5	 <p><b>Interactions</b></p> <ul style="list-style-type: none"> <li>van der Waals</li> <li>Conventional Hydrogen Bond</li> <li>Pi-Pi T-shaped</li> <li>Alkyl</li> <li>Pi-Alkyl</li> </ul>
SD36	−7.0	 <p><b>Interactions</b></p> <ul style="list-style-type: none"> <li>van der Waals</li> <li>Conventional Hydrogen Bond</li> <li>Pi-Alkyl</li> </ul>

(10 mg mL<sup>-1</sup>) against *E. coli*. On the other hand, the presence of 4-bromophenyl attached to the 6-acetyl naphthalene-2-sulfonamide shifted the activity towards the Gram-positive *S. aureus* with the best MIC (20 mg mL<sup>-1</sup>) among the tested compounds. Furthermore, it was concluded that the presence of any halogen at the *ortho*, *meta* or *para* position of the phenyl moiety or even pyridine-2-yl or pyridine-3-yl rings linked to the naphthalene-sulfonamide core structure switched on the activity towards *C. albicans*. The compounds that were strongly

effective against *Candida* were **5b**, **5d** and **5j**, with an MIC of 10 mg mL<sup>-1</sup> (S3 in SI).

**2.2.3.1 Minimum bactericidal concentration of the promising compounds (MBC).** The direct plating technique<sup>66</sup> was used to spread 100 µL of the minimum inhibitory concentration of the promising compounds onto XLD and Baird Parker agar for *E. coli* and *S. aureus*, and the plates were incubated at 44 °C and 37 °C/24 h, respectively. In contrast, for *C. albicans*, 100 µL of the negative cells were plated onto potato dextrose agar and



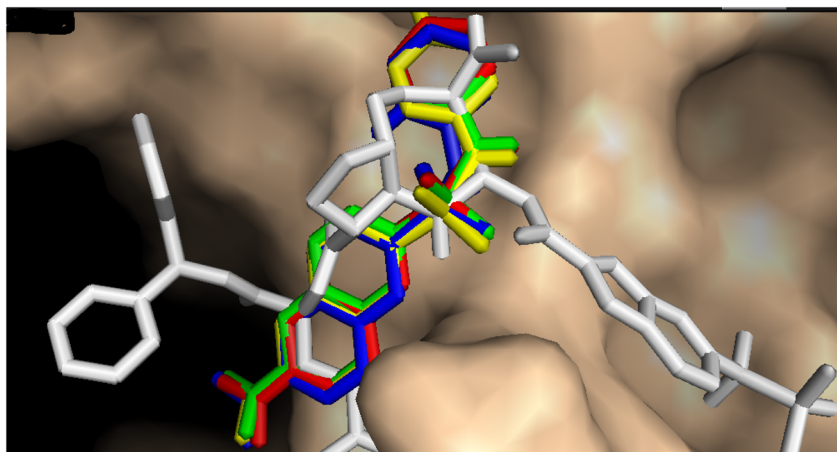


Fig. 6 The surface structure of the STAT-3 binding pocket showing the native ligand SD36 (white) superimposed with 5a (red), 5b (green), 5e (yellow), and 5i (blue).

incubated at 25 °C/72 h. The results revealed that the tested compounds had bactericidal and mycotoxin-inhibiting activity.

#### 2.2.4. *In vitro* enzymatic assay of the promising compounds

**2.2.4.1 Inhibition of STAT3 tyrosine phosphorylation.** ELISA was used to characterize the *in vitro* inhibitory activity against STAT3 phosphorylation of the four MCF7 anti-proliferative promising compounds 5a, 5b, 5e, 5i and cryptotanshinone as a reference, as shown in Table 4.<sup>67</sup> The best compound was 5e with  $IC_{50} = 3.01 \mu M$ , followed by 5b with  $IC_{50} = 3.59 \mu M$ , which were approximately half the values of the  $IC_{50}$  (7.87 and 8.58  $\mu M$ ) of 5e and 5i, respectively. Favorably, 5e and 5b were more potent as STAT3 inhibitors, exhibiting approximately 2-fold higher potency than the previously reported lead sulfonyl-*N*-(naphthalene-1-yl)acrylamide derivative (compound 1). This emphasized the importance of the presence of electron-withdrawing groups (Br and F) at the *para* position of the phenyl nucleus, which is attached to the sulfonamide moiety in the 6-acetyl-naphthalene core structure for the STAT3 phosphorylation inhibitory activity (S4 in the SI).

**2.2.4.2 Inhibition of bacterial topoisomerase II.** Commercially available topoisomerase II assay kits (Inspiralis Ltd, UK) were used to evaluate the antibacterial activity of the synthesized compounds through their ability to inhibit *E. coli* and *S. aureus* topoisomerases (gyrase and topoisomerase IV). The DNA gyrase supercoiling assay<sup>68,69</sup> and ATPase assay,<sup>69,70</sup> topoisomerase IV ATPase assay,<sup>69,70</sup> and cleavage assay were performed in *E. coli*,<sup>71,72</sup> while the decatenation assay was performed in *S. aureus*.<sup>69</sup> Tested compounds were dissolved in DMSO and added to each assay at different concentrations to determine the  $IC_{50}$  value.

**2.2.4.2.1 Inhibition of *E. coli* DNA gyrase and topoisomerase IV.** In Table 5, the enzymatic assay results of compound 5b showed moderate activities with nearly twice the value of  $IC_{50}$  of the corresponding reference drug, except for the topoisomerase IV cleavage assay, where it was 1.5-fold more potent than norfloxacin (S5 and S6 in the SI).

**2.2.4.2.2 Inhibition of *S. aureus* DNA gyrase and topoisomerase IV.** Table 5 summarizes the results of compound 5e, which showed approximately similar inhibitory activity to norfloxacin in the decatenation topoisomerase IV assay. Compound 5e possessed nearly twice the value of  $IC_{50}$  of the corresponding reference drug in the DNA gyrase supercoiling and ATPase assays. It also showed weaker activities (more than 3-fold less than ciprofloxacin) in the topoisomerase IV ATPase assay (S5 and S6 in the SI). It can be concluded that both 5b and 5e had remarkable inhibitory activity against topoisomerase IV in the cleavage and decatenation assays, respectively. Finally, both compounds might require some structural modification to improve their inhibitory activity against *E. coli* and *S. aureus* DNA gyrase and topoisomerase IV enzymes, respectively.

### 2.3. Computational study

**2.3.1. *In silico* prediction of drug likeness, ADME studies.** The compound is predicted to be an orally bioavailable candidate in accordance with its theoretically measured physico-chemical and pharmacokinetic parameters. The Swiss ADME website (<https://www.swissadme.ch>) was used to assess the drug-likeness and ADME properties for the final compounds 5a–5j, as shown in Tables 6 and 7. All of the tested compounds successfully passed the Lipinski rule of five without any violation.<sup>73</sup> The total polar surface area (TPSA) of each compound was evaluated and was within the required range between 20 and 130 Å<sup>2</sup>.<sup>74</sup> Concerning the lipophilicity,  $\log P_{o/w}$  represents the relative solubility of a compound in *n*-octanol (representing the cell membrane lipid bilayer) and water (as a model for fluids inside and outside the cell). Herein, we used MLOGP for the prediction of the compounds' lipophilicity, where all of the compounds fulfilled the acceptable lipophilicity range (<4.15), which guaranteed good oral and intestinal absorption.<sup>75</sup> Conversely, the water solubility was estimated from Ali classification, where all of the compounds possessed moderate solubility except 5h and 5i, which were water-soluble. Concerning the other pharmacokinetic parameters in Table 6,

**Table 9** The predicted binding affinity and 2D binding mode of **5b** in *E. coli* DNA gyrase and topoisomerase IV enzymes

Compounds	Binding affinity negative (kcal mol <sup>-1</sup> )	2D predicted binding mode representing the types and measurements of the binding interactions in the <i>E. coli</i> DNA gyrase (PDB 5L3j) binding pocket
<b>5b</b>	−7.2	
6G9 (native ligand)	−6.7	NA

**Interactions**

van der Waals

Conventional Hydrogen Bond

Pi-Anion

Pi-Sigma

Pi-Alkyl

Compound	Binding affinity negative (kcal mol <sup>-1</sup> )	2D predicted binding mode representing the types and measurements of the binding interactions in the <i>E. coli</i> topoisomerase IV (PDB 1S16) binding pocket
<b>5b</b>	−9.2	
ANP (native ligand)	−8.6	NA

**Interactions**

van der Waals

Conventional Hydrogen Bond

Halogen (Fluorine)

Pi-Cation

Pi-Sigma

Pi-Alkyl



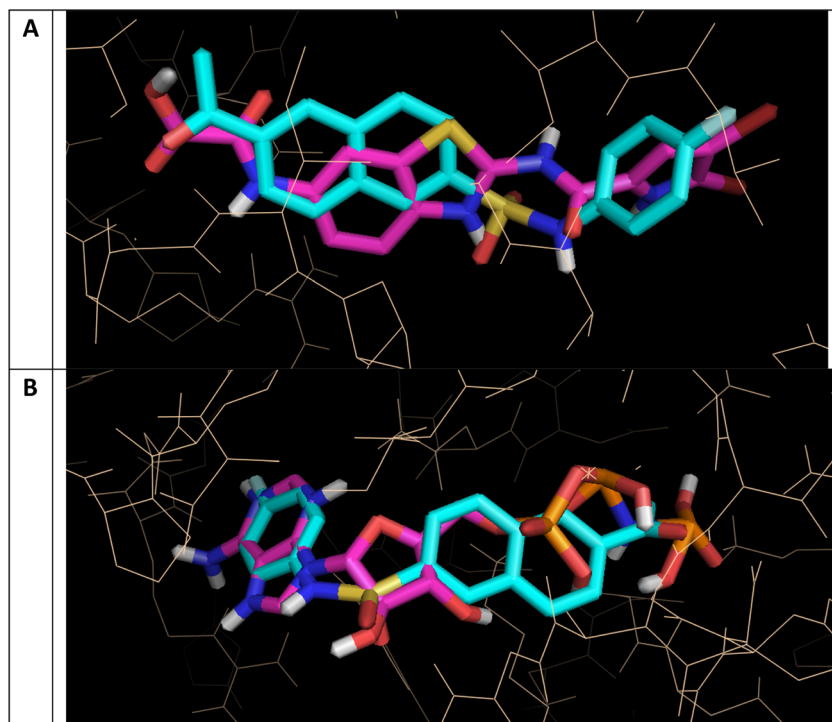


Fig. 7 (A) The compound **5b** (cyan) superimposed over the native ligand 6G9 (pink) in the binding pocket of *E. coli* DNA gyrase (sticks). (B) Compound **5b** (cyan) superimposed over the native ligand ANP (pink) in the *E. coli* topoisomerase IV binding pocket (sticks).

interestingly, all of the compounds were predicted to be passively absorbed from the gastrointestinal tract (GIT) and did not cross the blood–brain barrier, except for compound **5h**, which might be due to the presence of the *N*-benzyl moiety in its structure. The metabolism and elimination of the drugs as a protective mechanism for the body are controlled by several systems, including P-glycoprotein and CYP450.<sup>76</sup> None of the tested compounds were substrates for the active efflux across the cell membrane of the P-gp. Generally, the inhibitory effect of any drug on one or more of the CYP450 isoenzymes leads to drug–drug interactions and side effects due to its accumulation in the body.<sup>77</sup> The inhibitory profiles of the compounds **5a–5j** against CYP1A2, CYP2C19, CYP2C9, CYP2D6, and CYP3A4 are shown in Table 7.

**2.3.2. Molecular docking simulation study.** For deep exploration of the molecular interactions of the promising compounds in terms of their anticancer and antimicrobial activities, we selected compounds **5a**, **5b**, **5e**, and **5i** to be docked in the binding pocket of STAT-3 (PDB ID 6NJS).<sup>78</sup> We also selected compound **5b** to be docked in *E. coli* DNA gyrase (PDB ID 5L3j)<sup>79</sup> and topoisomerase IV (PDB ID 1S16).<sup>79</sup> For compound **5e**, it was docked in the binding pocket of *S. aureus* DNA gyrase (PDB ID 4URO)<sup>80</sup> and topoisomerase IV (PDB ID 4URN).<sup>80</sup> The 3D structures of the target proteins co-crystallized with their corresponding native ligands were downloaded from the Protein Data Bank (<https://www.rcsb.org/>). The molecular docking study was performed using Autodock Vina Wizard PyRx (<https://pyrx.sourceforge.io/>),<sup>81</sup> as previously reported.<sup>82</sup> The protein preparation involved the removal of the ions,

water, unnecessary chains, and the native ligand, then energy minimization was carried out using the YASARA energy minimization server.<sup>83</sup> Both the native ligand and the tested compounds were subjected to PyRx universal force field optimization and ligand preparation. Each native ligand was redocked in its target enzyme, where the RMSD values were 0.6 Å, 0.7 Å, 0.6 Å, 0.8 Å, and 0.7 Å, in order to ensure the validation of the docking study. Finally, for the 2D visualization of the binding interactions in the binding site of each enzyme, Biovia Discovery Studio 2024 (<https://discover.3ds.com/>) was used.

In Table 8, the binding scores of **5a**, **5b**, **5e**, and **5i** in STAT3 were very close to each other, but slightly less than that of the native ligand SD36. This might be explained due to the large molecular weight difference between SD36 and the four tested compounds. Consequently, all of them were superimposed over each other in the binding groove, but there was a part without interaction with our tested compounds, as depicted in Fig. 6. Interestingly, all of the tested compounds bound similarly to each other and with the same amino acid residues as SD36. Three favorable hydrogen bonds were formed between the O of the acetyl group with Gln 644, the O of SO<sub>2</sub> and Glu 638, and NH and Ser 636, in addition to other van der Waals and different pi interactions, as demonstrated. This emphasized the importance of both the 6-acetyl and 2-sulfonamide moieties, which are linked to the naphthalene core structure for its activity as STAT3 inhibitors, in addition to the essential presence of the 4-F-phenyl, 4-Br-phenyl, phenyl, and 2-pyridinyl moieties linked to sulfonamide, to ensure the activity of the compounds.



Table 10 The predicted binding affinity and 2D binding mode of **5e** in *S. aureus* DNA gyrase and topoisomerase IV enzymes

Compounds	Binding affinity negative (kcal mol <sup>-1</sup> )	2D predicted binding mode representing the types and measurement of the binding interactions in the <i>S. aureus</i> DNA gyrase (PDB 4URO) binding pocket
<b>5e</b>	−6.5	
Novobiocin	−6.9	NA
Compound	Binding affinity negative (kcal mol <sup>-1</sup> )	2D predicted binding mode representing the types and measurement of the binding interactions in the <i>S. aureus</i> topoisomerase IV (PDB 4UNR) binding pockets
<b>5e</b>	−9.4	
Novobiocin	−9.8	NA

Interestingly, the binding affinity of **5b** in *E. coli* DNA gyrase (PDB 5L3j) and topoisomerase IV (PDB 1S16) enzymes was predicted to be better than that of the native ligands 6G9 and ANP, respectively, as shown in Table 9. In the DNA gyrase, **5b**

acetyl formed two hydrogen bonds with Gly77 (2.46 Å) and Thr165 (2.68 Å), pi-anion with Glu50, pi-sigma with Ile94, pi-alkyl with Ile78 and Pro79, and van der Waals interactions. As depicted in Fig. 7A, our compound **5b** was typically





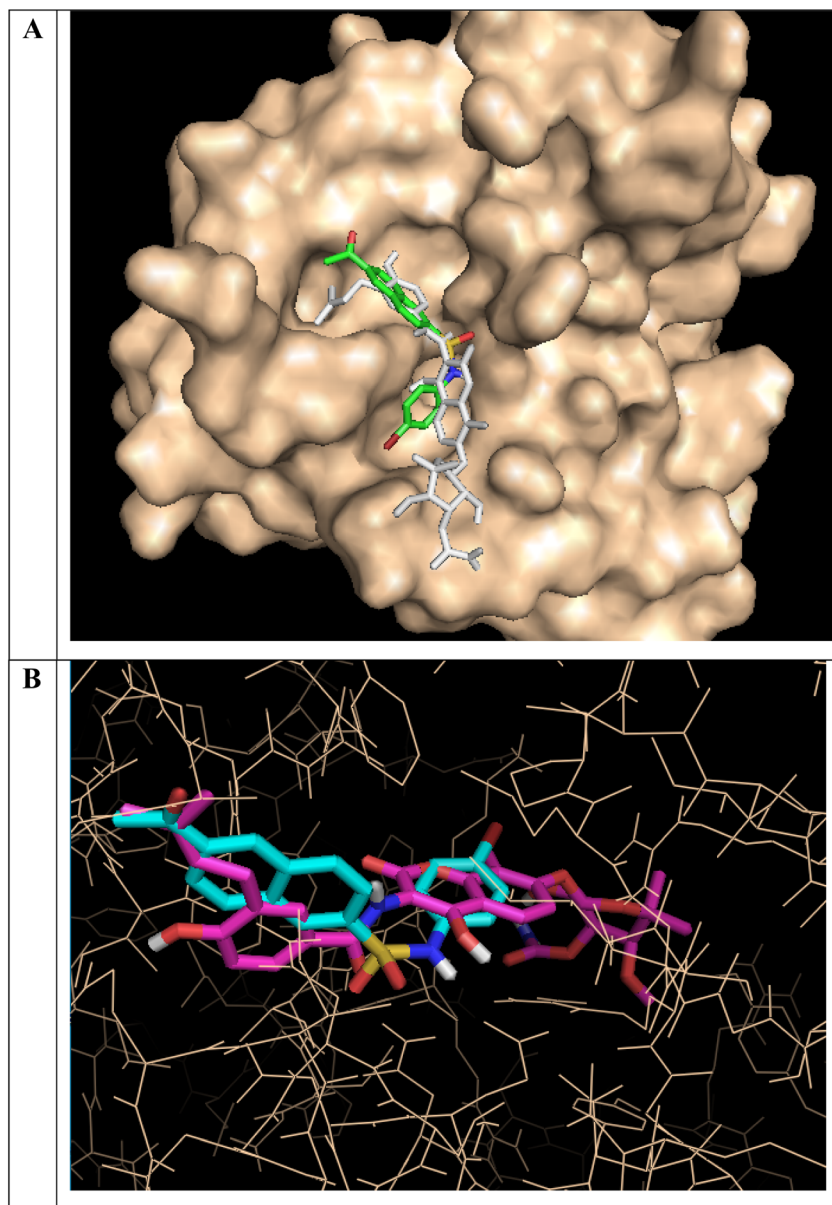


Fig. 8 (A) The compound **5e** (green) superimposed over the native ligand novobiocin (white) in the binding pocket of *S. aureus* DNA gyrase (surface). (B) Compound **5e** (cyan) superimposed over the native ligand novobiocin (pink) in the *S. aureus* topoisomerase IV binding pocket (sticks).

superimposed over the native ligand **6G9**. Conversely, in the topoisomerase IV binding pocket, **5b** was expected to form five hydrogen bonds, including the fluoro with Gly1073 (2.80 Å), O of SO<sub>2</sub> with Gly1098 (2.18 Å), and acetyl group O with Gly1113 (2.64 Å), Val1114 (2.11 Å) and Gly1115 (2.13 Å). There are also other van der Waals interactions, including pi-cation with Lys1098, pi-sigma with Met1074 and pi-alkyl with Pro1075, Ile1090. Compound **5b** was also superimposed over the native ligand ANP and interacted with the same amino acid residues, as shown in Fig. 7B.

In the *S. aureus* DNA gyrase (PDB 4URO) and topoisomerase IV (PDB 4URN) enzymes, the binding affinity of **5e** was predicted to be slightly less than that of the native ligand novobiocin, as

shown in Table 10. This might be attributed to the difference in the molecular size between **5e** and novobiocin. Thus, **5e** was superimposed over novobiocin in both enzymes but it did not occupy the whole binding cavity, as demonstrated in Fig. 8A and B. In *S. aureus* DNA gyrase, **5e** formed three hydrogen bonds, two of them with Asn54 (2.84 Å)/Ser128 (2.48 Å) and the two O atoms of SO<sub>2</sub>, and one with acetyl O and Tyr153 (2.42 Å). In addition to the van der Waals interactions, there were pi-sigma and two pi-alkyl interactions with Ile86 (3.76 Å, 4.30 Å, 5.02 Å, respectively), and finally 4-bromo formed an alkyl interaction with Pro87 (4.97 Å). In *S. aureus* topoisomerase IV, **5e** formed three hydrogen bonds as follows: NH with Glu53 (1.82 Å), the O atom of SO<sub>2</sub> with Asn56 (2.04 Å) and the O atom of acetyl with

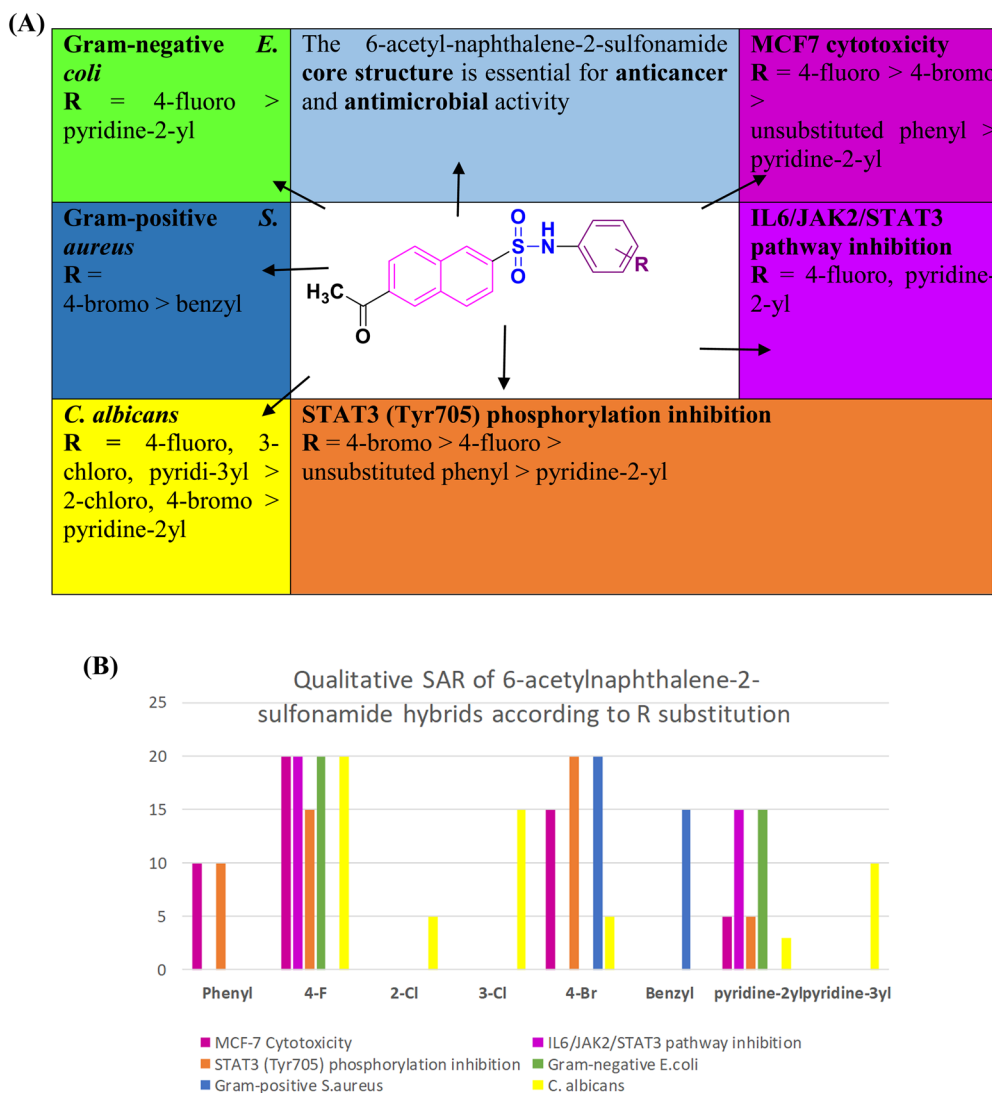


Fig. 9 (A) Summary of the SAR of naphthalene-2-sulfonamide hybrids. (B) An illustrative clustered column chart of the qualitative SAR of naphthalene-2-sulfonamide hybrids, highlighting the effect of R substituents in directing the biological activities.

Ala122 (2.07 Å). Also, the 4-bromo formed two alkyl interactions with Lys36 (4.31 Å) and Pro82 (4.05 Å) in addition to other van der Waals and pi-alkyl interactions.

The molecular docking study emphasized two major points. The first point is the flexibility of our 6-acetyl-naphthalene-2-sulfonamide core structure in fitting in STAT3 and bacterial (*E. coli* & *S. aureus*) DNA gyrase and topoisomerase IV, in which both the acetyl and sulfonamide moieties were predicted to form essential hydrogen bonds with crucial amino acid residues in the binding pockets of each target. The second point is the crucial role of *N*-aryl and/or heteroaryl substitution in directing the biological activity of our compounds.

A summary of the SAR of naphthalene-2-sulfonamide derivatives is illustrated in Fig. 9A and B, highlighting the descending order of different measured biological activities according to the substituted aryl or heteroaryl ring attached to the sulfonamide function group. Moreover, it emphasizes the 6-acetyl moiety and 2 sulfonamide moiety that were attached to the naphthalene core structure, and were responsible in

forming hydrogen bond interactions with essential amino acid residues in each target as predicted in the docking section.

### 3 Conclusion

In this study, multi-target and molecular hybridization drug design approaches were complementarily used in the synthesis of ten novel 6-acetylnaphthalene-2-sulfonamide hybrids (5a–5j) as anticancer (STAT3 inhibitors) and antimicrobial agents. All the compounds were assessed for anticancer activity against the MCF7 cell line. Compounds 5a, 5b, 5e, and 5i were shown to be more active agents against the MCF7 cell line. Among the investigated compounds, compounds 5b and 5i triggered apoptosis by the inhibition of the IL6/JAK2/STAT3 pathway, which in turn elevated the expression of the BAX and decreased the expression of the BCL2, Cyclin D1, and c-MYC target genes. The antimicrobial activity against *E. coli* (Gram-negative), *S. aureus* (Gram-positive), and *C. albicans* (fungal strain) was evaluated for the studied compounds. Then, the MIC was assessed for the



promising compounds (in AWDT) against the specific strains. The MIC values were in the range of 10–40 mg mL<sup>-1</sup>. This was followed by the evaluation of MBC, which emphasized the bactericidal and mycotic hindered effect of the tested compounds. Furthermore, *in vitro* enzymatic assays of the active compounds were performed against STAT3, *E. coli* (DNA gyrase/topoisomerase IV), and *S. aureus* (DNA gyrase/topoisomerase IV). The compounds **5e** and **5b** were very potent against STAT3 phosphorylation inhibition, with IC<sub>50</sub> values of 3.01 μM and 3.59 μM, respectively, which were more potent by approximately 2-fold than the previously reported sulfonyl-*N*-(naphthalene-1-yl) acrylamide lead derivative (compound **1**). Compound **5b** in *E. coli* potently inhibited topoisomerase IV (IC<sub>50</sub> = 5.3 μg mL<sup>-1</sup>) and moderately inhibited DNA gyrase (IC<sub>50</sub> = 7.07 μg mL<sup>-1</sup>) in comparison with the norfloxacin reference drug. In *S. aureus*, compound **5e** effectively inhibited topoisomerase IV (IC<sub>50</sub> = 7.65 μg mL<sup>-1</sup>) and moderately inhibited DNA gyrase (IC<sub>50</sub> = 8.83 μg mL<sup>-1</sup>) when compared with norfloxacin as a reference drug. The computational study demonstrated the good drug likeness and ADME profile of **5a–5j**. The molecular docking study of the promising compounds also revealed the favourable binding affinity and binding interactions of the native ligands in each specific target. A summary of the structure–activity relationship of the promising compounds was discussed in detail, which highlighted the flexibility of our core structure in fitting within the selected targets, in addition to the essential role of the *N*-aryl and/or heteroaryl R substitution in directing the biological activity of each compound towards a specific target. The whole series of 6-acetylnaphthalene-2-sulfonamide hybrids could be considered as building blocks that can be subjected to further modifications through QSAR-guided synthesis for improvement in their anti-cancer and antimicrobial activities. Therefore, future research should be focused on biological assessment to include resistant microbial strains, other cancer types, *in vivo* effectiveness, experimental ADME, toxicity investigations, and the exploration of synergistic effects with well-established therapeutic medicines.

## 4 Experimental

### 4.1. Chemistry

**4.1.1. Procedure for the synthesis of 6-acetylnaphthalene-2-sulfonyl chloride (3).** 2-Acetylnaphthalene (1.0 g) was treated with chlorosulfonic acid (5 mL) with continuous stirring for 2 h on an ice bath. After that, the ice bath was removed, and the mixture of the reaction was added slowly on ice to yield a white precipitate. Then, the precipitate was filtered and washed with distilled water several times until it was acid-free and crystallized from DCM to give white needles.

**4.1.2. General procedure for the synthesis of 6-acetyl-*N*-phenylnaphthalene-2-sulfonamide derivatives (5a–j).** An appropriate quantity of amine (1.5 mmol) was added to 6-acetylnaphthalene-2-sulfonyl chloride (1.0 mmol) in dichloromethane (DCM, 20 mL) for 1–3 h with continuous stirring at room temperature. After that, the precipitate was filtered and crystallized from ethanol to give the final product.

**4.1.2.1 6-Acetyl-*N*-phenylnaphthalene-2-sulfonamide (5a).** Yield 98%; mp 218–220 °C; IR:  $\nu$ /cm<sup>-1</sup>: 3220 (NH), 1668 (C=O);

<sup>1</sup>H NMR (500 MHz, DMSO-*d*<sub>6</sub>):  $\delta$ /ppm = 2.68 (s, 3H, CH<sub>3</sub>), 7.23–7.28 (m, 5H, Ar), 7.66 (t, 1H,  $J_{\text{HH}}$  = 15.25 Hz, Ar), 8.12 (d, 1H,  $J_{\text{HH}}$  = 8.55 Hz, Ar), 8.29 (d, 1H,  $J_{\text{HH}}$  = 7.15 Hz, Ar), 8.35 (d, 1H,  $J_{\text{HH}}$  = 10.00 Hz, Ar), 8.81 (d, 2H,  $J_{\text{HH}}$  = 9.05 Hz, Ar), 10.78 (s, 1H, NH). <sup>13</sup>C NMR (125 MHz, DMSO-*d*<sub>6</sub>):  $\delta$ /ppm: 27.28 (CH<sub>3</sub>), 112.15, 119.89, 120.61, 124.39, 125.41, 125.96, 126.07, 129.60, 129.92, 130.15, 138.09 (C-aromatics) and 198.17 (C=O). MS (EI, 70 eV):  $m/z$  326 [M<sup>+</sup>]. Anal. calcd for C<sub>18</sub>H<sub>15</sub>NO<sub>3</sub>S (325.38): C, 66.44; H, 4.65; N, 4.30; S, 9.85; found: C, 66.43; H 4.63; N, 4.29; S, 9.83%.

**4.1.2.2 6-Acetyl-*N*-(4-fluorophenyl)naphthalene-2-sulfonamide (5b).** Yield 94%; mp 228–230 °C; IR:  $\nu$ /cm<sup>-1</sup>: 3240 (NH), 1665 (C=O); <sup>1</sup>H NMR (500 MHz, DMSO-*d*<sub>6</sub>):  $\delta$ /ppm = 2.69 (s, 3H, CH<sub>3</sub>), 6.87–7.00 (m, 4H, Ar), 7.66 (t, 1H,  $J_{\text{HH}}$  = 7.85 Hz, Ar), 8.12 (s, 1H, Ar), 8.23 (d, 1H,  $J_{\text{HH}}$  = 9.64 Hz, Ar), 8.38 (d, 1H,  $J_{\text{HH}}$  = 8.10 Hz, Ar), 8.76 (d, 2H,  $J_{\text{HH}}$  = 9.55 Hz, Ar). <sup>13</sup>C NMR (125 MHz, DMSO-*d*<sub>6</sub>):  $\delta$ /ppm = 27.24 (CH<sub>3</sub>), 116.32, 116.41, 116.50, 121.20, 122.70, 125.97, 126.08, 136.17, 157.75, 159.65, 160.35 (C-aromatics), 198.19 (C=O). MS (EI, 70 eV):  $m/z$  343 [M<sup>+</sup>]. Anal. calcd for C<sub>18</sub>H<sub>14</sub>FN<sub>2</sub>O<sub>3</sub>S (343.37): C, 62.96; H, 4.11; N, 4.08; S, 9.34; found: C, 62.90; H 4.00; N, 4.07; S, 9.32%.

**4.1.2.3 6-Acetyl-*N*-(2-chlorophenyl)naphthalene-2-sulfonamide (5c).** Yield 86%; mp 180–182 °C; IR:  $\nu$ /cm<sup>-1</sup>: 3252 (NH), 1671 (C=O); <sup>1</sup>H NMR (500 MHz, DMSO-*d*<sub>6</sub>):  $\delta$ /ppm = 2.69 (s, 3H, CH<sub>3</sub>), 7.20–7.27 (m, 4H, Ar), 7.63 (t, 1H,  $J_{\text{HH}}$  = 7.15 Hz, Ar), 8.06 (d, 1H,  $J_{\text{HH}}$  = 9.05 Hz, Ar), 8.11 (d, 1H,  $J_{\text{HH}}$  = 7.15 Hz, Ar), 8.40 (d, 1H,  $J_{\text{HH}}$  = 8.10 Hz, Ar), 8.75 (t, 2H,  $J_{\text{HH}}$  = 7.88 Hz, Ar), 10.37 (s, 1H, NH). <sup>13</sup>C NMR (125 MHz, DMSO-*d*<sub>6</sub>):  $\delta$ /ppm = 27.30 (CH<sub>3</sub>), 121.81, 123.73, 125.06, 128.40, 128.65, 130.30, 136.21 (C aromatics), 198.25 (C=O). MS (EI, 70 eV):  $m/z$  359 [M<sup>+</sup>]. Anal. calcd for C<sub>18</sub>H<sub>14</sub>ClNO<sub>3</sub>S (359.83): C, 60.08; H, 3.92; N, 3.89; found: C, 60.06; H; 3.91; N, 3.89%.

**4.1.2.4 6-Acetyl-*N*-(3-chlorophenyl)naphthalene-2-sulfonamide (5d).** Yield 97%; mp 272–274 °C; IR:  $\nu$ /cm<sup>-1</sup>: 3223 (NH), 1665 (C=O); <sup>1</sup>H NMR (500 MHz, DMSO-*d*<sub>6</sub>):  $\delta$ /ppm = 2.69 (s, 3H, CH<sub>3</sub>), 6.96 (d, 1H,  $J_{\text{HH}}$  = 7.15 Hz, Ar), 7.00–7.12 (m, 3H, Ar), 7.13 (s, 1H, Ar), 7.71 (t, 1H, Ar), 8.22 (m, 1H, Ar), 8.33 (d, 1H,  $J_{\text{HH}}$  = 7.65 Hz, Ar), 8.41 (d, 1H,  $J_{\text{HH}}$  = 8.10 Hz, Ar), 8.74 (t, 2H,  $J_{\text{HH}}$  = 9.80 Hz, Ar), 11.05 (s, 1H, NH). <sup>13</sup>C NMR (125 MHz, DMSO-*d*<sub>6</sub>):  $\delta$ /ppm = 27.30 (CH<sub>3</sub>), 117.73, 118.80, 123.97, 125.09, 126.06, 126.32, 126.61, 128.83, 129.98, 131.44, 131.63, 132.69, 133.90, 134.90, 134.63, 135.14, 136.27, 139.49 (C aromatics), 198.07 (C=O). MS (EI, 70 eV):  $m/z$  360 [M<sup>+</sup>]. Anal. calcd for C<sub>18</sub>H<sub>14</sub>ClNO<sub>3</sub>S (361.84): C, 59.75; H, 4.46; N, 3.87; found: C, 59.74; H; 4.46; N, 3.86%.

**4.1.2.5 6-Acetyl-*N*-(4-bromophenyl)naphthalene-2-sulfonamide (5e).** Yield 98%; mp > 300 °C; IR:  $\nu$ /cm<sup>-1</sup>: 3220 (NH), 1666 (C=O); <sup>1</sup>H NMR (500 MHz, DMSO-*d*<sub>6</sub>):  $\delta$ /ppm = 2.68 (s, 3H, CH<sub>3</sub>), 7.31 (d, 2H,  $J_{\text{HH}}$  = 8.60 Hz, Ar), 7.50 (d, 2H,  $J_{\text{HH}}$  = 8.10 Hz, Ar), 7.68 (t, 1H,  $J$  = 7.50 Hz, Ar), 8.33 (d, 1H,  $J_{\text{HH}}$  = 7.65 Hz, Ar), 8.41 (d, 1H,  $J_{\text{HH}}$  = 8.10 Hz, Ar), 8.33 (d, 1H,  $J_{\text{HH}}$  = 7.15 Hz, Ar), 8.76 (d, 2H,  $J_{\text{HH}}$  = 8.15 Hz, Ar). MS (EI, 70 eV):  $m/z$  405 [M<sup>+</sup>]. Anal. calcd for C<sub>18</sub>H<sub>14</sub>BrNO<sub>3</sub>S (404.28): C, 53.48; H, 3.49; N, 3.46; found: C, 53.47; H; 3.48; N, 3.46%.

**4.1.2.6 6-Acetyl-*N*-(*o*-tolyl)naphthalene-2-sulfonamide (5f).** Yield 90%; mp 216–218 °C; IR:  $\nu$ /cm<sup>-1</sup>: 3282 (NH), 1667 (C=O); <sup>1</sup>H NMR (500 MHz, DMSO-*d*<sub>6</sub>):  $\delta$ /ppm = 1.83 (s, 3H, CH<sub>3</sub>), 2.70 (s, 3H, CH<sub>3</sub>), 6.96–7.06 (m, 4H, Ar), 7.65 (d, 1H,  $J_{\text{HH}}$  = 7.60 Hz,





Ar), 8.07–8.08 (m, 2H, Ar), 8.40–8.41 (m, 1H, Ar), 8.79 (d, 2H,  $J_{\text{HH}} = 7.50$  Hz, Ar), 9.95 (s, 1H, NH).  $^{13}\text{C}$  NMR (125 MHz, DMSO- $d_6$ ):  $\delta/\text{ppm} = 18.10$  ( $\text{CH}_3$ ), 27.28 ( $\text{COCH}_3$ ), 119.67, 123.31, 125.11, 126.84, 126.90, 127.04, 127.09, 127.28, 127.52, 130.29, 131.19, 131.61, 131.78, 138.26 (C aromatics), 198.20 (C=O). MS (EI, 70 eV):  $m/z$  338 [ $\text{M}^-$ ]. Anal. calcd for  $\text{C}_{19}\text{H}_{17}\text{NO}_3\text{S}$  (339.41): C, 67.24; H, 5.05; N, 4.13; found: C, 67.24; H, 5.00; N, 4.12%.

**4.1.2.7 6-Acetyl-N-(4-methoxyphenyl)naphthalene-2-sulfonamide (5g).** Yield 80%; mp 208–210 °C; IR:  $\nu/\text{cm}^{-1}$ : 3245 (NH), 1665 (C=O);  $^1\text{H}$  NMR (500 MHz, DMSO- $d_6$ ):  $\delta/\text{ppm} = 2.69$  (s, 3H,  $\text{CH}_3$ ), 3.63 (s, 3H,  $\text{OCH}_3$ ), 6.67 (d, 2H,  $J_{\text{HH}} = 7.15$  Hz, Ar), 6.84 (d, 2H,  $J_{\text{HH}} = 7.15$  Hz, Ar), 7.64 (d, 1H,  $J_{\text{HH}} = 6.20$  Hz, Ar), 8.14 (t, 2H,  $J_{\text{HH}} = 10.72$  Hz, Ar), 8.22 (s, 1H, Ar), 8.77 (d, 2H,  $J_{\text{HH}} = 9.05$  Hz, Ar), 9.95 (s, 1H, NH).  $^{13}\text{C}$  NMR (125 MHz, DMSO- $d_6$ ):  $\delta/\text{ppm} = 27.27$  ( $\text{CH}_3$ ), 55.93 ( $\text{OCH}_3$ ), 114.82, 115.31, 122.30, 123.51, 125.48, 125.94, 131.56, 132.39, 136.24, 156.98 (C aromatics), 198.20 (C=O). MS (EI, 70 eV):  $m/z$  354 [ $\text{M}^-$ ]. Anal. calcd for  $\text{C}_{19}\text{H}_{17}\text{NO}_4\text{S}$  (355.41): C, 64.21; H, 4.82; N, 3.94; found: C, 64.20; H, 4.82; N, 3.93%.

**4.1.2.8 6-Acetyl-N-benzyl-naphthalene-2-sulfonamide (5h).** Yield 70%; mp 217–219 °C; IR:  $\nu/\text{cm}^{-1}$ : 3250 (NH), 1668 (C=O);  $^1\text{H}$  NMR (500 MHz, DMSO- $d_6$ ):  $\delta/\text{ppm} = 2.70$  (s, 3H,  $\text{CH}_3$ ), 4.74 (s, 2H,  $\text{CH}_2$ ), 7.37–7.47 (m, 5H, Ar), 8.10–8.76 (m, 6H, Ar). MS (EI, 70 eV):  $m/z$  340 [ $\text{M}^+$ ]. Anal. calcd for  $\text{C}_{19}\text{H}_{17}\text{NO}_3\text{S}$  (339.41): C, 67.24; H, 5.05; N, 4.13; found: C, 67.23; H, 5.00; N, 4.12%.

**4.1.2.9 6-Acetyl-N-(pyridin-2-yl)naphthalene-2-sulfonamide (5i).** Yield 67%; mp 240–242 °C; IR:  $\nu/\text{cm}^{-1}$ : 3245 (NH), 1678 (C=O);  $^1\text{H}$  NMR (500 MHz, DMSO- $d_6$ ):  $\delta/\text{ppm} = 2.67$  (s, 3H,  $\text{CH}_3$ ), 6.71 (t, 1H,  $J_{\text{HH}} = 7.56$  Hz, Ar), 7.69 (t, 3H,  $J_{\text{HH}} = 6.88$  Hz, Ar), 8.07 (d, 1H,  $J_{\text{HH}} = 9.05$  Hz, Ar), 8.34 (t, 2H,  $J_{\text{HH}} = 11.20$  Hz, Ar), 8.70 (s, 1H, Ar), 8.86 (d, 2H,  $J_{\text{HH}} = 9.05$  Hz, Ar), 12.91 (s, 1H, NH).  $^{13}\text{C}$  NMR (125 MHz, DMSO- $d_6$ ):  $\delta/\text{ppm} = 27.54$  ( $\text{CH}_3$ ), 113.93, 115.40, 125.38, 126.00, 126.76, 130.42, 130.63, 131.21, 134.93, 154.84 (C aromatics), 198.21 (C=O). MS (EI, 70 eV):  $m/z$  326 [ $\text{M}^+$ ]. Anal. calcd for  $\text{C}_{17}\text{H}_{14}\text{N}_2\text{O}_3\text{S}$  (326.37): C, 62.56; H, 4.32; N, 8.58; found: C, 64.55; H, 4.31; N, 8.57%.

**4.1.2.10 6-Acetyl-N-(pyridin-3-yl)naphthalene-2-sulfonamide (5j).** Yield 68%; mp 222–224 °C; IR:  $\nu/\text{cm}^{-1}$ : 3224 (NH), 1664 (C=O);  $^1\text{H}$  NMR (500 MHz, DMSO- $d_6$ ):  $\delta/\text{ppm} = 2.67$  (s, 3H,  $\text{CH}_3$ ), 7.61 (d, 1H,  $J_{\text{HH}} = 7.80$  Hz, Ar), 7.65 (d, 1H,  $J_{\text{HH}} = 7.88$  Hz, Ar), 7.66 (t, 1H,  $J_{\text{HH}} = 7.50$  Hz, Ar), 8.15 (d, 2H,  $J_{\text{HH}} = 10.45$  Hz, Ar), 8.22 (s, 1H, Ar), 8.34 (t, 2H,  $J_{\text{HH}} = 7.87$  Hz, Ar), 8.76 (t, 2H,  $J_{\text{HH}} = 7.87$  Hz, Ar), 11.05 (s, 1H, NH).  $^{13}\text{C}$  NMR (125 MHz, DMSO- $d_6$ ):  $\delta/\text{ppm} = 27.27$  ( $\text{CH}_3$ ), 124.46, 125.09, 126.04, 126.32, 127.01, 131.64, 132.71, 136.74, 141.40, 145.46 (C aromatics), 198.04 (C=O). MS (EI, 70 eV):  $m/z$  326 [ $\text{M}^+$ ]. Anal. calcd for  $\text{C}_{17}\text{H}_{14}\text{N}_2\text{O}_3\text{S}$  (326.37): C, 62.56; H, 4.32; N, 8.58; found: C, 64.54; H, 4.30; N, 8.57%.

## 4.2. Biology

**4.2.1. Cell culture.** Cancer cells (MCF7 cells) and normal cells (MDCK cells) were purchased from the American Type Culture Collection (ATCC) and kept under the appropriate conditions. The cells were cultivated in Dulbecco's Modified Eagle's Medium (DMEM) (Lonza, Belgium) at 37 °C in a humidified incubator with 5%  $\text{CO}_2$ , supplemented with 10%

fetal bovine serum (FBS), 100 U  $\text{mL}^{-1}$  penicillin, and 100  $\mu\text{g}/\text{mL}$  streptomycin sulphate. Following trypsinization (0.025% trypsin and 0.02% EDTA), the cells were collected and twice washed with Dulbecco's phosphate-buffered saline (DPBS). Cells were divided for continued cultivation when the cell density approached 80%. Cells in the logarithmic growth phase were used for the experiments.

**4.2.2. Neutral red uptake assay.** The neutral red uptake test was used to assess the cytotoxicity of different compounds.<sup>84</sup> The capability of viable cells to absorb and bind the supravital dye neutral red in the lysosomes is the basis for the neutral red uptake test, which offers a quantitative estimate of the number of viable cells in a culture. MCF7 and MDCK cells were treated with various concentrations of the test compounds (12.5, 25, 50, and 100  $\mu\text{M}$ ) and were incubated at a density of  $10^4$  cells per well of a 96 well plate for 48 hours. The neutral red working solution (0.4  $\mu\text{g mL}^{-1}$ ) from Sigma-Aldrich was incubated at 37 °C for 24 h, similarly to the treated cells. Neutral red medium (100  $\mu\text{L}$ ) was added to each well of the cultured cells after the culture media were withdrawn, and the cells were incubated for two hours to allow the pivotal dye to be incorporated into the live cells. After the neutral red media were decanted, 150  $\mu\text{L}$  of Dulbecco's PBS buffer was added to each well. A micrometer plate shaker was used to rapidly agitate the cells for at least 10 minutes after adding 150  $\mu\text{L}$  of extraction buffer (1% acetic acid, 50% ethanol (96%), and 49% deionized  $\text{H}_2\text{O}$ ) to extract the dye from the cells. Using a micro-liter plate reader spectrophotometer (Sorin, Biomedica A., Milan, Italy), the extract neutral red color intensity was evaluated at 450 and 630 nm as the excitation and emission wavelengths, respectively. The relationship between the utilized log concentrations and the neutral red intensity value was used to estimate the  $\text{IC}_{50}$  of the investigated compound. Instead of adding the test compound, the medium was supplied to the untreated cells (negative control). Doxorubicin (Dox,  $\text{Mr} = 543.5$ ) as a positive control and cytotoxic natural compound was tested, which provided 100% inhibition. The studied compound was dissolved in DMSO (dimethyl sulfoxide), and its final concentration was less than 0.2% in the cells. Each test and analysis were carried out three times, and the results were averaged.

**4.2.3. Selectivity index (SI).** The cytotoxic selectivity (*i.e.*, safety) of the tested compounds against cancer cells, in contrast to normal cells, is shown by the selectivity index (SI), which was estimated using the tested compound  $\text{IC}_{50}$  in normal cells *versus* cancer cells.<sup>85</sup>

**4.2.4. Quantitative real-time PCR (qRT-PCR) analysis.** Using the RNeasy Mini Kit (Qiagen, Germany), RNA was extracted from MCF7 cells ( $3 \times 10^4$  cells per well) after a 48 hour treatment. The concentration and purity of the extracted RNA were measured using the NanoDrop One Microvolume UV spectrophotometer (Thermo Fisher Scientific, USA). The RevertAid First Strand cDNA Synthesis Kit (Thermo Fisher Scientific, USA) was used to convert RNA from each treatment to first-strand cDNA in accordance with the manufacturer's instructions. Sequences of specific primers are presented in Table 11. Using the Maxima SYBR Green qPCR Master Mix (2X) (Thermo Fisher Scientific, USA), the expression levels of IL6,



Table 11 Primers for qRT-PCR analysis

Gene	Primer forward (5'-3')	Primer reverse (5'-3')
$\beta$ -Actin	CCTTCCTGGGCATGGAGTCCT	GGAGCAATGATCTTGATCTTC
IL6	GGTACATCCTCGACGGCATCT	GTGCCTCTTTGCTGCTTTCAC
JAK2	CCAGATGGAACTGTTCGCTCAG	GAGGTTGTACATCAGAAACACC
STAT3	TGAGACTTGGGCTTACCATTGGGT	TCTTTAATGGGCCACAACAGGGCT
BCL2	CCTGGTGGACAACATCGCC	AATCAAACAGAGGCCGCATGC
BAX	GATGCGTCCACCAAGAAG	AGTTGAAGTTGCCGTCAG
Cyclin D1	GAGGAAGAGGAGGAGGAGGA	GAGATGGAAGGGGAAAGAG
c-MYC	GCTGCTTAGACGCTGGATT	TAACGTTGAGGGGCATCG

JAK2, STAT3, BCL2, BAX, Cyclin D1, and c-MYC genes were normalized relative to the  $\beta$ -Actin transcript, and the  $2^{-\Delta\Delta C_T}$  methodology was used to measure these values.<sup>86</sup> For a total of 40 cycles of amplification, the reaction conditions were as follows: 95 °C for 10 min, 95 °C for 15 s, 60 °C for 30 s, and 72 °C for 30 s. Estimation of the gene expression was measured using the DNA Technology Detecting Thermocycler DT Lite 4S1 (Russia).

**4.2.5. Antimicrobial screening assay and MIC.** The agar well diffusion test (AWDT) was used for the tested compounds against a variety of certified reference strains, including Gram-negative *E. coli* O157 ATCC 700728, Gram-positive *S. aureus* ATCC 25923, and mycotic reference strain/isolate, including yeast, *C. albicans* ATCC 10231, and mould isolate; *A. flavus*, as was previously reported.<sup>87</sup> The promising compounds were chosen to investigate their minimum inhibitory concentration (MIC) against a specific strain, according to a previously reported method,<sup>65</sup> for the determination of the bactericidal effect.<sup>66</sup>

#### 4.2.6. In vitro enzymatic assay of the promising compounds

**4.2.6.1 STAT3 phosphorylation kit.** Phospho-Stat3 (Tyr705) ELISA kit (Cell Signaling Technology, USA)<sup>67</sup> was used according to the manufacturer's instructions at eight different dilutions of the four tested compounds (100, 30, 10, 3, 1, 0.3, 0.1, and 0.03  $\mu$ M).

**4.2.6.2 DNA gyrase supercoiling assay (Inspiralis kit).** In this assay, the substrate is the relaxed pRB322, which is supercoiled by gyrase. The two forms of plasmid, either relaxed or supercoiled, could be separated by agarose gel, following the manufacturer's instructions and as previously reported.<sup>68,69</sup>

**4.2.6.3 Gyrase and topoisomerase IV ATPase assay (Inspiralis kit).** Gyrase requires energy from ATP hydrolysis to make negative supercoils in DNA, in addition to topoisomerase IV energy from ATP hydrolysis. This assay links ATP hydrolysis to the conversion of NADH to NAD<sup>+</sup>, which can be measured by a change in absorbance at 340 nm. The Inspiralis gyrase/topoisomerase IV ATPase kits for *S. aureus* and *E. coli* were used following the manufacturer's instructions and as previously reported.<sup>69,70</sup>

**4.2.6.4 S. aureus topoisomerase IV decatenation assay (Inspiralis kit).** The substrate in this assay is interlinked double-stranded kinetoplast DNA, which can be decatenated by topoisomerase IV, releasing minicircles from this network. These minicircles migrate into the gel (in gel electrophoresis), which

can be visualized after staining with ethidium bromide. The kit was used following the manufacturer's instructions and as previously reported.<sup>69</sup>

**4.2.6.5 E. coli topoisomerase IV cleavage assay (Inspiralis kit).** Topoisomerase IV makes a double-strand break in DNA (cleavage complex), then passes another DNA segment and reseals the break. Some inhibitors for the enzyme stabilize the cleavage complex. In this assay, the substrate is supercoiled pBR322. The relaxed and supercoiled forms can be separated by gel electrophoresis, following the manufacturer's instructions and as previously reported.<sup>71,72</sup>

**4.2.7. Statistics.** The data are shown as the mean  $\pm$  standard error mean (SEM). IC<sub>50</sub> values are determined using SigmaPlot version 11. The data analysis and significant differences between the studied compounds were analyzed using the Student's *t*-test. As statistically significant, the value of *P* < 0.05 was used. Every data set was repeatable.

## Author contributions

Ghada H. Elsayed: conceptualization, data curation, formal analysis, investigation, methodology of anticancer effect and gene expression, resources, validation, writing original draft, writing – review & editing; Nagwa M. Abdelazeem: conceptualization, data curation, investigation, methodology, resources, validation, visualization; Alaa M. Saleh: data curation, formal analysis, investigation, methodology, validation, writing original draft; Sherein Abd El-Moez: investigation, methodology, resources, validation; Marwa El-Hussieny: conceptualization, data curation, formal analysis, investigation, methodology, resources, validation, writing original draft; Aisha A. K. Al-Ashmawy: conceptualization, data curation, formal analysis, investigation, methodology, resources, software, validation, visualization, writing original draft, writing – review & editing.

## Conflicts of interest

No conflicts of interest (financially and non-financially) or personal relationships influencing the reported work were declared by the authors in this paper.

## Data availability

The data supporting this article have been included as part of the SI file, which can be found in the online version.



Supplementary information: S1 and S2 spectra of final compounds, S3 AWDI figures, S4 STAT3 phosphorylation inhibition graphs, S5 and S6 *E. coli* and *S. aureus* DNA gyrase and topoisomerase *in vitro* enzymatic assay graphs and methodology. See DOI: <https://doi.org/10.1039/d5ra05413c>.

## Acknowledgements

The authors would like to thank the National Research Centre for providing the equipment and facilities to carry out this practical work.

## References

- H. Sung, J. Ferlay, R. L. Siegel, M. Laversanne, I. Soerjomataram, A. Jemal and F. Bray, *Ca-Cancer J. Clin.*, 2021, **71**, 209–249.
- M. Liu, H. Li, H. Zhang, H. Zhou, T. Jiao, M. Feng, F. Na, M. Sun, M. Zhao, L. Xue and L. Xu, *Cell Death Dis.*, 2022, **13**, 287.
- H. Li, P. Yang, J. H. Wang, J. Zhang, Q. Ma, Y. Jiang, Y. Wu, T. Han and D. Xiang, *J. Hematol. Oncol.*, 2022, **15**, 2.
- J. H. Kang, M. J. Li, P. P. Luan, D. K. Jiang, Y. W. Chen, X. Xu, Q. Yu, Y. W. Xu, Q. Su, W. H. Peng and W. X. Jian, *Cell Biol. Int.*, 2020, **44**, 2053–2064.
- X. Zhang, F. Hu, G. Li, G. Li, X. Yang, L. Liu, R. Zhang, B. Zhang and Y. Feng, *Cell Death Dis.*, 2018, **9**, 25.
- X. Fang, Y. Hong, L. Dai, Y. Qian, C. Zhu, B. Wu and S. Li, *Mol. Carcinog.*, 2017, **56**, 2434–2445.
- B. Kim, H. S. Kim, S. Kim, G. Haegeman, B. K. Tsang, D. N. Dhanasekaran and Y. S. Song, *Cancer Res. Treat.*, 2017, **49**, 338–349.
- C. Sun, J. Yang, H. B. Cheng, W. X. Shen, Z. Q. Jiang, M. J. Wu, L. Li, W. T. Li, T. T. Chen, X. W. Rao, J. R. Zhou and M. H. Wu, *Phytomedicine*, 2019, **61**, 152848.
- X. Zhang, H. Lu, W. Hong, L. Liu, S. Wang, M. Zhou, B. Chen and Y. Bai, *Oncol. Rep.*, 2018, **39**, 1892–1900.
- J. Chen, Y. Wei, W. Yang, Q. Huang, Y. Chen, K. Zeng and J. Chen, *Front. Oncol.*, 2022, **12**, 903800.
- J. I. Song and J. R. Grandis, *Oncogene*, 2000, **19**, 2489–2495.
- G. I. Karaliotas, K. Mavridis, A. Scorilas and G. C. Babis, *Mol. Med. Rep.*, 2015, **12**, 4514–4521.
- N. Ragimov, A. Krauskopf, N. Navot, V. Rotter, M. Oren and Y. Aloni, *Oncogene*, 1993, **8**, 1183–1193.
- L. R. Thomas and W. P. Tansey, *Open Access J. Sci. Technol.*, 2015, **3**, 26.
- S. J. Riedl and Y. Shi, *Nat. Rev. Mol. Cell Biol.*, 2004, **5**, 897–907.
- D. Sinibaldi, W. Wharton, J. Turkson, T. Bowman, W. J. Pledger and R. Jove, *Oncogene*, 2000, **19**, 5419–5427.
- J. P. Alao, *Mol. Cancer*, 2007, **6**, 24.
- J. Chun, K. Song and Y. S. Kim, *Phytother. Res.*, 2018, **32**, 2501–2509.
- Q. Xie, Z. Yang, X. Huang, Z. Zhang, J. Li, J. Ju, H. Zhang and J. Ma, *J. Hematol. Oncol.*, 2019, **12**, 60.
- J. H. Ma, L. Qin and X. Li, *Cell Commun. Signaling*, 2020, **18**, 33.
- N. Gohil, R. Ramírez-García, H. Panchasara, S. Patel, G. Bhattacharjee and V. Singh, *Front. Cell. Infect. Microbiol.*, 2018, **8**, 106.
- <https://www.who.int/news/item/29-04-2019-new-report-calls-for-urgent-action-to-avert-antimicrobial-resistance-crisis>.
- <https://www.who.int/news/item/27-02-2017-who-publishes-list-of-bacteria-for-which-new-antibiotics-are-urgently-needed>.
- G. S. Bisacchi and J. I. Manchester, *ACS Infect. Dis.*, 2015, **1**, 4–41.
- J. M. Thomas, *Notes Rec. R. Soc. Lond.*, 1992, **46**, 317–323.
- K. Vogel, J. Sterling, Y. Herzig and A. Nudelman, *Tetrahedron*, 1996, **52**, 3049–3056.
- G. Wang, W. Liu, J. Tang, X. Ma, Z. Gong, Y. Huang, Y. Li and Z. Peng, *Bioorg. Chem.*, 2020, **104**, 104265.
- Y. Y. Chen, L. Gopala, R. R. Y. Bheemanaboina, H. B. Liu, Y. Cheng, R. X. Geng and C. H. Zhou, *ACS Med. Chem. Lett.*, 2017, **8**, 1331–1335.
- A. K. Debnath, L. Radigan and S. Jiang, *J. Med. Chem.*, 1999, **42**, 3203–3209.
- A. C. Goudie, L. M. Gaster, A. W. Lake, C. J. Rose, P. C. Freeman, B. O. Hughes and D. Miller, *J. Med. Chem.*, 1978, **21**, 1260–1264.
- S. Biswas, S. Zhang, F. Fernandez, B. Ghosh, J. Zhen and E. Kuzhikandathil, *J. Med. Chem.*, 2007, **51**, 101–117.
- J. X. Di and H. Y. Zhang, *Anticancer Drugs*, 2019, **30**, 846–853.
- X. Wang, Y. Lu, D. Sun, J. Qian, S. Tu, W. Yue, H. Lin, H. Tang, F. Meng, Q. He, Z. Xie, Y. Zhang, H. Chen, S. Ma, Z. Zuo and F. Ye, *Bioorg. Chem.*, 2022, **125**, 105864.
- F. Y. Chang, J. E. Peacock, D. M. Musher, P. Triplett, B. B. MacDonald, J. M. Mylotte, A. O'Donnell, M. M. Wagener and V. L. Yu, *Medicine*, 2003, **82**, 333–339.
- N. S. Ryder, I. Frank and M. C. Dupont, *Antimicrob. Agents Chemother.*, 1986, **29**, 858–860.
- J. M. Mühlbacher, *Clin. Dermatol.*, 1991, **9**, 479–485.
- R. Kalariya, V. Pandya, N. Gohil, G. Bhattacharjee, V. Singh, D. P. Rajani, R. Bhosale and J. S. Yadav, *Eur. J. Med. Chem. Rep.*, 2022, **6**, 100078.
- H. Yoshino, N. Ueda, J. Nijima, H. Sugumi, Y. Kotake, N. Koyanagi, K. Yoshimatsu, M. Asada, T. Watanabe, T. Nagasu, K. Tsukahara, A. Iijima and K. Kitoh, *J. Med. Chem.*, 1992, **35**, 2496–2497.
- S. S. Stokes, R. Albert, E. T. Buurman, B. Andrews, A. B. Shapiro, O. M. Green, A. R. McKenzie and L. R. Otterbein, *Bioorg. Med. Chem. Lett.*, 2012, **22**, 7019–7023.
- I. R. Ezabadi, C. Camoutsis, P. Zoumpoulakis, A. Geronikaki, M. Soković, J. Glamočilić and A. Ćirić, *Bioorg. Med. Chem.*, 2008, **16**, 1150–1161.
- C. T. Supuran, A. Casini and A. Scozzafava, *Med. Res. Rev.*, 2003, **23**, 535–558.
- A. M. Mauer, E. E. W. Cohen, P. C. Ma, M. F. Kozloff, L. Schwartzberg, A. I. Coates, J. Qian, A. E. Hagey and G. B. Gordon, *J. Thorac. Oncol.*, 2008, **3**, 631–636.
- S. Apaydin and M. Török, *Bioorg. Med. Chem. Lett.*, 2019, **29**, 2042–2050.





- 44 A. Więckowska, M. Kołaczkowski, A. Bucki, J. Godyń, M. Marcinkowska, K. Więckowski, P. Zaręba, A. Siwek, G. Kazek, M. Głuch-Lutwin, P. Mierzejewski, P. Bienkowski, H. Sienkiewicz-Jarosz, D. Knez, T. Wichur, S. Gobec and B. Malawska, *Eur. J. Med. Chem.*, 2016, **124**, 63–81.
- 45 N. M. Abdelazeem, W. M. Aboulthana, Z. A. Elshahid, M. El-Hussieny and A. A. K. Al-Ashmawy, *J. Mol. Struct.*, 2024, **1310**, 138224.
- 46 A. M. Alfayomy, S. A. Abdel-Aziz, A. A. Marzouk, M. S. A. Shaykoon, A. Narumi, H. Konno, S. M. Abou-Seri and F. A. F. Ragab, *Bioorg. Chem.*, 2021, **108**, 104555.
- 47 M. Mihara, M. Hashizume, H. Yoshida, M. Suzuki and M. Shiina, *Clin. Sci.*, 2012, **122**, 143–159.
- 48 J. Gyamfi, Y. H. Lee, M. Eom and J. Choi, *Sci. Rep.*, 2018, **8**, 8859.
- 49 E. Bousoik and H. Montazeri Aliabadi, *Front. Oncol.*, 2018, **8**, 287.
- 50 K. Leslie, C. Lang, G. Devgan, J. Azare, M. Berishaj, W. Gerald, Y. B. Kim, K. Paz, J. E. Darnell, C. Albanese, T. Sakamaki, R. Pestell and J. Bromberg, *Cancer Res.*, 2006, **66**, 2544–2552.
- 51 P. J. Real, A. Sierra, A. De Juan, J. C. Segovia, J. M. Lopez-Vega and J. L. Fernandez-Luna, *Oncogene*, 2002, **21**, 7611–7618.
- 52 F. C. Hsieh, G. Cheng and J. Lin, *Biochem. Biophys. Res. Commun.*, 2005, **335**, 292–299.
- 53 S. Kunigal, S. S. Lakka, P. K. Sodadasu, N. Estes and J. S. Rao, *Int. J. Oncol.*, 2009, **34**, 1209–1220.
- 54 Z. W. Liang, B. F. Guo, Y. Li, X. J. Li, X. Li, L. J. Zhao, L. F. Gao, H. Yu, X. J. Zhao, L. Zhang and B. X. Yang, *Asian J. Androl.*, 2011, **13**, 481–486.
- 55 G. Niu, K. L. Wright, Y. Ma, G. M. Wright, M. Huang, R. Irby, J. Briggs, J. Karras, W. D. Cress, D. Pardoll, R. Jove, J. Chen and H. Yu, *Mol. Cell. Biol.*, 2005, **25**, 7432–7440.
- 56 E. Bousoik, P. Mahdipoor, A. Alhazza and H. Montazeri Aliabadi, *Eur. J. Pharm. Sci.*, 2022, **175**, 106233.
- 57 Y. Guo, F. Xu, T. Lu, Z. Duan and Z. Zhang, *Cancer Treat. Rev.*, 2012, **38**, 904–910.
- 58 J. H. Ma, L. Qin and X. Li, *Cell Commun. Signaling*, 2020, **18**, 33.
- 59 X. Wang, W. Qiu, G. Zhang, S. Xu, Q. Gao and Z. Yang, *Int. J. Clin. Exp. Pathol.*, 2015, **8**, 5017–5025.
- 60 B. Huang, X. Lang and X. Li, *Front. Oncol.*, 2022, **12**, 1023177.
- 61 G. H. Elsayed, A. M. Fahim and A. I. Khodair, *J. Mol. Struct.*, 2022, **1265**, 133401.
- 62 Z. Yang, H. Xu, Y. Yang, C. Duan, P. Zhang, Y. Wang, K. Fu, Y. Shen and M. X. Xu, *Breast Cancer Res. Treat.*, 2023, **197**, 255–267.
- 63 M. B. Minus, H. Wang, J. O. Munoz, A. M. Stevens, A. E. Mangubat-Medina, M. J. Krueger, W. Liu, M. M. Kasembeli, J. C. Cooper, M. I. Kolosov, D. J. Twardy, M. S. Redell and Z. T. Ball, *Org. Biomol. Chem.*, 2020, **18**, 3288–3296.
- 64 S. Schwarz, A. Böttner, H. M. Hafez, C. Kehrenberg, M. Kietzmann, D. Klarmann, G. Klein, P. Krabisch, T. Kühn, G. Luhofer, A. Richter, W. Traeder, K.-H. Waldmann, J. Wallmann and C. Werckenthin, *Berl. Munch. Tierarztl. Wochenschr.*, 2003, **116**(9–10), 353–361.
- 65 J. M. Andrews, *J. Antimicrob. Chemother.*, 2001, **48**, 5–16.
- 66 G. L. French, *J. Antimicrob. Chemother.*, 2006, **58**, 1107–1117.
- 67 X. Wang, Y. Lu, D. Sun, J. Qian, S. Tu, W. Yue, H. Lin, H. Tang, F. Meng, Q. He, Z. Xie, Y. Zhang, H. Chen, S. Ma, Z. Zuo and F. Ye, *Bioorg. Chem.*, 2022, **125**, 105864.
- 68 Ž. Jakopin, J. Ilaš, M. Barančoková, M. Brvar, P. Tammela, M. Sollner Dolenc, T. Tomašič and D. Kikelj, *Eur. J. Med. Chem.*, 2017, **130**, 171–184.
- 69 W. A. Zagahary, M. M. Anwar, S. S. Abd El-Karim, G. E. A. Awad, G. K. Hussein and N. M. Mahfouz, *Egypt. J. Chem.*, 2021, **64**, 3817–3839.
- 70 M. Gjorgjieva, T. Tomašič, M. Barančokova, S. Katsamakas, J. Ilaš, P. Tammela, L. P. Mašič and D. Kikelj, *J. Med. Chem.*, 2016, **59**, 8941–8954.
- 71 S. Alt, L. A. Mitchenall, A. Maxwell and L. Heide, *J. Antimicrob. Chemother.*, 2011, **66**, 2061–2069.
- 72 H. H. H. Mohammed, S. H. Abbas, E. S. M. N. Abdelhafez, J. M. Berger, S. Mitarai, M. Arai and G. E. D. A. A. Abu-Rahma, *Monatsh. Chem.*, 2019, **150**, 1809–1824.
- 73 C. A. Lipinski, F. Lombardo, B. W. Dominy and P. J. Feeney, *Adv. Drug Delivery Rev.*, 2012, **64**, 4–17.
- 74 P. Ertl, B. Rohde and P. Selzer, *J. Med. Chem.*, 2000, **43**, 3714–3717.
- 75 A. Daina, O. Michielin and V. Zoete, *Sci. Rep.*, 2017, **7**, 1–13.
- 76 R. A. B. van Waterschoot and A. H. Schinkel, *Pharmacol. Rev.*, 2011, **63**, 390–410.
- 77 J. Kirchmair, A. Göller, D. Lang, J. Kunze, B. Testa, I. D. Wilson, R. C. Glen and G. Schneider, *Nat. Rev. Drug Discovery*, 2015, **14**, 387–404.
- 78 L. Bai, H. Zhou, R. Xu, Y. Zhao, K. Chinnaswamy, D. Mceachern, J. Chen, C. Yang, Z. Liu, M. Wang, L. Liu, H. Jiang, B. Wen, J. L. Meagher, D. Sun, J. Stuckey and S. Wang, *Cancer Cell*, 2019, **36**, 498–511.
- 79 S. Bellon, J. D. Parsons, Y. Wei, K. Hayakawa, L. L. Swenson, P. S. Charifson, J. A. Lippke, R. Aldape and C. H. Gross, *Antimicrob. Agents Chemother.*, 2004, **48**, 1856–1864.
- 80 J. Lu, S. Patel, N. Sharma, S. M. Soisson, R. Kishii, M. Takei, Y. Fukuda, K. J. Lumb and S. B. Singh, *ACS Chem. Biol.*, 2014, **9**, 2023–2031.
- 81 O. Trott and A. J. Olson, *J. Comput. Chem.*, 2010, **31**, 455–461.
- 82 A. A. K. Al-Ashmawy, M. Abdelraof, A. Saleh and A. M. Srou, *Drug Dev. Res.*, 2025, **86**, e70122.
- 83 E. Krieger, K. Joo, J. Lee, J. Lee, S. Raman, J. Thompson, M. Tyka, D. Baker and K. Karplus, *Proteins*, 2009, **77**, 114–122.
- 84 G. Repetto, A. del Peso and J. L. Zurita, *Nat. Protoc.*, 2008, **3**, 1125–1131.
- 85 P. Prayong, S. Barusrux and N. Weerapreeyakul, *Fitoterapia*, 2008, **79**, 598–601.
- 86 K. J. Livak and T. D. Schmittgen, *Methods*, 2001, **25**, 402–408.
- 87 E. Pinho, L. Magalhães, M. Henriques and R. Oliveira, *Ann. Microbiol.*, 2011, **61**, 493–498.

